

Contour Integral Methods for time treatment in Reduced Basis Methods

Nicola Guglielmi*

Mattia Manucci†

January 6, 2022

Abstract

In this paper we discuss a reduced basis method for linear evolution PDEs, which is based on the application of the Laplace transform. The main advantage of this approach consists in the fact that, differently from time stepping methods, like Runge-Kutta integrators, the Laplace transform allows to compute the solution directly at a given instant, which can be done by approximating the contour integral associated to the inverse Laplace transform by a suitable quadrature formula. In terms of the reduced basis methodology, this determines a significant improvement in the reduction phase - like the one based on the classical proper orthogonal decomposition (POD) - since the number of vectors to which the decomposition applies is drastically reduced as it does not contain all intermediate solutions generated along an integration grid by a time stepping method. We show the effectiveness of the method by some illustrative parabolic PDEs arising from finance and also provide some evidence that the method we propose, when applied to a simple advection equation, does not suffer the problem of slow decay of singular values which instead affects methods based on time integration of the Cauchy problem arising from space discretization.

Keywords: contour integral methods, reduced basis methods, parametric partial differential equation, evolutionary PDEs, weighted pseudospectra, inverse Laplace transform, convection-diffusion equations.

AMS subject classifications: 65L05, 65R10, 65J10, 65M20, 65M99.

1 Introduction

Parametrized partial differential equations (PPDEs) occur in many contexts such as industrial or financial applications. They are solved by means of high-fidelity (or full-order) approximation techniques such as finite elements, finite volumes, finite differences or spectral methods. However, the use of high-fidelity approximation techniques may become prohibitive when they are required

*Gran Sasso Science Institute, via Crispi 7, L'Aquila, Italy. Email: nicola.guglielmi@gssi.it

†Gran Sasso Science Institute, via Crispi 7, L'Aquila, Italy. Email: mattia.manucci@gssi.it

to deal quickly and efficiently with the repetitive solution of PPDEs.

For this class of problems, *reduced-order modeling* – also named *model order reduction* – is a generic expression used to identify any approach aimed at replacing the high-fidelity problem by one featuring with a much lower numerical complexity, introducing a controllable error with respect to the high-fidelity solution. The assumption on which the *reduced-order model* (ROM) techniques are based is that the behaviour of a possibly complex system can be described by a small number of dominant modes.

In particular, among the reduced-order modeling techniques, a remarkable instance is represented by the *reduced basis* (RB) methods. The strategy is to solve, during a computationally onerous *offline* phase, the high-fidelity problem only for few instances of the input parameters, aiming to construct a set of base solutions, the so called *reduced base*. This *reduced space* is usually of much smaller dimension with respect to the solution space associated to the high fidelity problem. After that, for every new instance of the input parameters, the associated solution is approximated by a suitable linear combination of the base elements of the reduced space. The unknown coefficients of this combination are obtained during the *online* phase by solving a reduced problem generated through a Galerkin projection onto the reduced space.

In this work we are interested in time-dependent problems and their treatment in the reduced basis context. A survey on this topic is given in [9] where two methodologies are described and compared. The first one, and probably the one considered “standard”, is based upon a time stepping solver in the offline phase. The reduced basis is then usually formed by the POD-Greedy method [7, 13]. The drawback of these time-stepping schemes is that, in order to approximate the solution at a certain time $T = t_n$, one needs to compute an approximation of the solution, for both the full and reduced problem, at grid points $0 < t_1 < t_2 < \dots < t_n$, which would be particularly demanding if T is large. The second approach consists in treating time as an additional variable. This results in a problem of dimension $d + 1$ where d denotes the spatial dimension. The reduced basis is formed by a standard Greedy algorithm and then the full problem is Galerkin projected to the reduced space [30]. It is well known that the size of the discrete problems grows exponentially with respect to the numbers of variables when keeping the same accuracy (the so-called curse of dimensionality), therefore the computational cost for this approach can easily become prohibitive.

We introduce a new strategy to address time dependence in the reduced basis context. It consists of employing a contour integral method (see e.g. [11, 12]) to numerically invert the Laplace transform as time integrator for the full and reduced problem. This time solver is indicated when one is interested to determine the solution at a specific time T or even in certain time window $[t_0, t_1]$. We will show that the new approach is very efficient when compared to the standard methodologies. Moreover our method can be extended to efficiently perform the reduction in linear hyperbolic problems which are known to be challenging for the standard reduced basis method [26, 10].

The article is organized as follows. In Section 2 we present the mathematical formulation of contour integral methods and reduced basis method. In Section 3 we describe two types of greedy searches based on the new time integrator. In Section 4 numerical experiments are presented for: 1) the Black-Scholes model, 2) the Heston model and 3) a simple linear advection problem with discontinuous initial data. Finally in Section 5 we state few conclusions.

2 Problem formulation

We consider convection diffusion PPDEs of the form

$$\begin{aligned} \frac{\partial U}{\partial t}(x, t; \mu) &= \mathcal{A}(x; \mu)U(x, t; \mu) + f(x, t; \mu), \quad x \in \Omega, \quad t \in (0, T], \\ &+ \text{B.C.} \\ U(x, 0; \mu) &= U_0(x; \mu) \end{aligned} \quad (1)$$

with \mathcal{A} a linear second order differential operator, Ω bounded domain, $T \in \mathbb{R}^+$ and $\mu \in \mathcal{D} \subset \mathbb{R}^d$ a vector containing the parameters of the problem with \mathcal{D} closed set. We assume that the problem is well defined and that it admits a unique solution. Given a suitable discretization in space we end up with the Cauchy problem

$$\dot{u}(t) = A(\mu)u(t) + b(t; \mu), \quad t > 0, \quad u(0; \mu) = u_0(\mu) = U_0(\mu), \quad (2)$$

with $A(\mu)$ discretized operator of size N_h and $b(t; \mu)$ a source term possibly including boundary conditions.

Note that, despite our focus is on parabolic problems, we also briefly discuss applications of our methodology to a simple hyperbolic problem.

2.1 The numerical inverse Laplace transform

In order to approximate the solution $u(t; \mu)$ to (2) it is possible to derive methods based on the Laplace transform and its numerical inversion, which do not require a time grid. We assume the existence of the Laplace transform of $b(t; \mu)$ and that it admits a bounded analytic extension to a suitable region of the complex plane. We then apply the Laplace transform to (2), which yields

$$\hat{u}(z; \mu) = (zI - A(\mu))^{-1} \left(u_0 + \hat{b}(z; \mu) \right), \quad (3)$$

where $\hat{b} = \mathcal{L}(b)$ and I stands for the identity matrix.

Then we can obtain the solution u at time t by considering the inverse Laplace transform

$$u(t; \mu) = \frac{1}{2\pi i} \int_{\Gamma} e^{zt} \hat{u}(z; \mu) dz, \quad (4)$$

being the contour Γ an open piecewise smooth curve running from $-i\infty$ to $+i\infty$ and surrounding all singularities of $\hat{b}(\mu)$ and the eigenvalues of $A(\mu)$, $\forall \mu \in \mathcal{D}$. To approximate the Bromwich integral (4), we parameterize the integration contour Γ by a suitable map $z = z(x)$, $x \in \mathbb{R}$, so that

$$u(t; \mu) = \frac{1}{2\pi i} \int_{\Gamma} e^{zt} \hat{u}(z; \mu) dz = \frac{1}{2\pi i} \int_{\mathbb{R}} G(x; \mu) dx,$$

with

$$G(x; \mu) = e^{z(x)t} \hat{u}(z(x); \mu) z'(x). \quad (5)$$

Since we are interested in approximating $u(t)$ within precision tol , we will only consider the portion of the Bromwich integral parameterized in a closed interval,

$$I = \frac{1}{2\pi i} \int_{\mathbb{R}} G(x; \mu) dx \approx \frac{1}{2\pi i} \int_{-c\pi}^{c\pi} G(x; \mu) dx, \quad (6)$$

for a suitable truncation parameter $c \in (0, c_{\max})$, which we determine by the estimate

$$|G(c\pi; \mu)| = tol$$

for tol the desired accuracy.

The application of a quadrature formula to approximate (6) provides a numerical approximation of u , at the given time t without need of computing it at intermediate time instants. For instance, an application of the trapezoidal rule provides the desired approximation

$$I_N = \frac{c}{iN} \sum_{j=1}^{N-1} G(\xi_j, \mu), \quad (7)$$

$$\text{with } \xi_j = -c\pi + j \frac{2c\pi}{N}, \quad j = 1, \dots, N-1. \quad (8)$$

Under some regularity assumption on $G(x, \mu)$ it can be shown (see Theorem 1 in [11]) that the trapezoidal quadrature rule has an exponential rate of convergence with respect to number of quadrature nodes N .

The crucial point is the construction of the contour integral Γ and its parametrization. Assuming that the Laplace transform can be analytically extended to the left half of the complex plane and that this extension is properly bounded with respect to z , several authors have proposed different contour profiles and parametrizations for Γ . We refer the reader to the recent article [11] for a detailed review of the literature concerning the choice of the profile Γ .

The magnitude of the resolvent norm $\|(zI - A(\mu))^{-1}\|$ (with $\|\cdot\|$ being the spectral norm when not indicated differently) has a crucial role in the rate of convergence of any contour integral method based on Laplace transform. Due to this, the choice and parametrization of the integration contour requires some information on the behaviour of the resolvent norm. In a recent work [12] elliptic, parabolic and hyperbolic profiles have been proposed, in connection to the knowledge of the so-called weighted ϵ -pseudospectrum of A (see [29])

$$\sigma_{\epsilon, t}(A) = \left\{ z \in \mathbb{C} : e^{-\text{Re}(z)t} \sigma_{\min}(A - zI) \leq \epsilon \right\}$$

for suitable $\epsilon > 0$ and with σ_{\min} denoting the smallest singular value.

Since A is in general non-normal, due to the convection terms in the operator \mathcal{A} , the pseudospectrum may rapidly increase around the spectrum of A , making the problem quite challenging.

2.2 The Kolmogorov n -width

Given the vector of parameters μ we define the map

$$\Phi : \mu \longrightarrow u(x, T; \mu), \quad (9)$$

with $u(x, T; \mu)$ solution of (1) with parameters μ at time $t = T$, and the associated solution manifold

$$\mathcal{M} = \{u(x, T; \mu) \mid \mu \in \mathcal{D}\} \subset \mathbb{V} \quad (10)$$

where \mathbb{V} is the space to which the solution belongs $\forall \mu \in \mathcal{D}$. In practise, we work with the map associated to the discrete problem

$$\Phi_h : \mu \longrightarrow u(T; \mu),$$

with $u(T; \mu)$ solution of (2) at time $t = T$. The corresponding solution manifold is

$$\mathcal{M}_h = \{u(T; \mu) \mid \mu \in \mathcal{D}\} \subset \mathbb{V}_{N_h}$$

where \mathbb{V}_{N_h} is the vector space of dimension N_h to which the discrete solution belongs. Due to the isomorphism among vector spaces with the same finite dimension, it is not restrictive to identify \mathbb{V}_{N_h} with \mathbb{R}^{N_h} and $\|\cdot\|_{\mathbb{V}_{N_h}}$ with the standard ℓ^2 -norm.

The Kolmogorov n -width of \mathcal{M}_h is defined as

$$d_n(\mathcal{M}_h) := \inf_{\dim(Y)=n} \sup_{u \in \mathcal{M}_h} \text{dist}(u, Y), \quad (11)$$

where the infimum is taken over all n -dimensional subspaces Y of \mathbb{V}_{N_h} , see [14]. Hence, (11) measures how well the manifold \mathcal{M}_h can be approximated by some n -dimensional space Y of dimension $n \leq N_h$. If the n -width decays rapidly as n increases, for instance $d_n(\mathcal{M}_h) \approx O(e^{-n})$, it indicates that the solution manifold can be well approximated by a space of dimension $n \ll N_h$, i.e. what is called reduced space.

The fact that the Kolmogorov n -width decays fast is problem-specific, i.e., not all problems exhibit this behaviour. Up to our knowledge there does not exist a general theory which, given a PPDE and the associated solution manifold, is able to determine the behaviour of its n -width. However, there are rigorous results for certain classes of problems. For instance in [10] it is shown that $d_n(\mathcal{M}_h) = O(n^{-1/2})$ for initial-boundary value problems of the 1d-hyperbolic wave equation with discontinuous initial data, that is consistent with the known slow decay of $d_n(\mathcal{M}_h)$ for the linear transport problem [26]. For these problems the polynomial decay is due to the moving discontinuity whose location changes with respect to the parametric velocity of the wave. Another important result is stated in [5] where it is shown the exponential decay of (11) under the hypothesis of holomorphicity of the map (9). One significant contribution of this work is a result on the Kolmogorov n -width behavior for problems of type (1), which is presented in the following theorem.

Theorem 1. *Given problem (1), under the hypothesis*

- $\mathcal{A}(\mu) : D \rightarrow I$, with $I \subseteq D$, is a linear bounded second order differential operator $\forall \mu \in \mathcal{D}$;
- $U_0(x; \mu) \in C^\infty(\bar{\Omega}) \forall \mu \in \mathcal{D}$;
- $f(x, t; \mu) \in L^\infty\left(C^\infty(\bar{\Omega}), (0, T]\right) \forall \mu \in \mathcal{D}$;

there exist an n^* such that, for $n > n^*$, the Kolmogorov n -width associated to the solution manifold (10) has an exponential decay, that is, for suitable constants c_1, c_2 ,

$$d_n(\mathcal{M}) \leq c_1 e^{-c_2 n}; \quad n > n^* \quad (12)$$

Proof. See appendix A. □

In order to recover an exponential decay behaviour for the Kolmogorov n -width, Theorem 1 requires linearity on the space operator and smoothness in space of the initial and source terms. The conditions are quite restrictive and far from being necessary. Indeed it is known that there are non-linear space operators that exhibit exponential decay of the n -width (see e.g. [5]). On the other hand these conditions, given a problem of type (1), are easy to be checked. Note that the results for linear hyperbolic problems [10, 26] do not contrast with the statement of Theorem 1 since they refer to linear boundary value problems of hyperbolic type with discontinuous initial data.

2.3 The reduced problem

We aim to apply the reduced basis method to problem (2) where the time integration is performed through the contour integral method proposed in [12]. For a detailed survey on reduced basis methods starting from the framework of the continuum problem, we remand to [14].

First, we observe that the solution given by (7), is a linear combination of the function $G(x; \mu)$ evaluated on the quadrature points ξ_j defined as in (8), for $j = 1, \dots, N - 1$. Therefore, recalling (5) and the fact that $\hat{u}(z(\xi_j); \mu) \in \mathbb{C}^{N_h}$, for all j and μ , we define the solution manifold of our problem as the set

$$\mathcal{M}_h = \left\{ \hat{u}(z(\xi_j); \mu) \mid \mu \in \mathcal{D}, j = 1, \dots, N - 1 \right\}. \quad (13)$$

In Section 3 we will discuss how to build an appropriate low dimensional subspace of \mathcal{M}_h but for the moment we simply assume that such a space has been constructed. We can uniquely represent the reduced space by the N_r base vectors $\zeta_i \in \mathbb{C}^{N_h}$, with $i = 1, \dots, N_r$, N_r possibly much smaller than N_h . The $N - 1$ reduced solutions are linear combinations of such base vectors and are determined by the Galerkin projection of (3) onto the reduced space, that means

$$\hat{u}_r(z_j; \mu) = \sum_{i=1}^{N_r} \beta_{j,i}(\mu) \zeta_i$$

satisfying

$$\langle (z_j I - A(\mu)) \hat{u}_r(z_j), \zeta_i \rangle = \langle u_0 + \hat{b}(z_j; \mu), \zeta_i \rangle \quad \text{for } i = 1, \dots, N_r \quad (14)$$

where $\langle \cdot, \cdot \rangle$ denotes the scalar product on \mathbb{C}^{N_h} and $z_j = z(\xi_j)$.

Thanks to Galerkin orthogonality we can make use of the C ea's Lemma to connect the best ap-

proximation error with the reduced approximation:

$$\begin{aligned} \max_{1 \leq j \leq N-1} \left\| \hat{u}(z_j; \mu) - \hat{u}_r(z_j; \mu) \right\| &\leq \max_{1 \leq j \leq N-1} \left(\left(1 + \frac{\gamma_j(\mu)}{\alpha_j(\mu)} \right) \inf_{v \in \mathbb{C}^{N_r}} \left\| \hat{u}(z_j; \mu) - v \right\| \right) \\ &\leq d_{N_r}(\mathcal{M}_h) \max_{1 \leq j \leq N-1} \left(1 + \frac{\gamma_j(\mu)}{\alpha_j(\mu)} \right); \end{aligned} \quad (15)$$

where $\alpha_j(\mu)$ and $\gamma_j(\mu)$ are respectively the coercivity and continuity constants of $z_j I - A(\mu)$, i.e.

$$\begin{aligned} \alpha_j(\mu) &= \min_{\|w\|=1} w^T (z_j I - A(\mu)) w; \\ \gamma_j(\mu) &= \max_{\|w\|=1} \max_{\|y\|=1} y^T (z_j I - A(\mu)) w. \end{aligned}$$

Thus, the quality of the reduced basis approximation, based on a Galerkin projection, depends, as is well known, on the coercivity and continuity constants of the operators $z_j I - A(\mu)$, which are problem-dependent. Furthermore, the quality also depends on the accuracy of the reduced basis space in approximating the entire solution manifold.

Once $\hat{u}_r(z_j)$ is computed for all $j = 1, \dots, N-1$ we can reconstruct the solution of the reduced problem in the time domain as

$$u_r(t; \mu) = \frac{c}{iN} \sum_{j=1}^{N-1} e^{z_j t} \hat{u}_r(z_j; \mu) z_j'; \quad (16)$$

where $z_j' = \frac{d}{dx} z(x)|_{x=\xi_j}$. Its reliability with respect to the high fidelity solution is ensured by (15)

$$\begin{aligned} \left\| u(t; \mu) - u_r(t; \mu) \right\| &= \left\| \frac{c}{iN} \sum_{j=1}^{N-1} e^{z_j t} \left(\hat{u}(z_j; \mu) - \hat{u}_r(z_j; \mu) \right) z_j' \right\| \\ &\leq \frac{c}{N} \sum_{j=1}^{N-1} \left(e^{\operatorname{Re}(z_j) t} |z_j'| \left\| \hat{u}(z_j; \mu) - \hat{u}_r(z_j; \mu) \right\| \right) \\ &\leq d_{N_r}(\mathcal{M}_h) \frac{c}{N} \sum_{j=1}^{N-1} \left(e^{\operatorname{Re}(z_j) t} |z_j'| \left(1 + \frac{\gamma_j(\mu)}{\alpha_j(\mu)} \right) \right). \end{aligned}$$

Note that the reduced space lies in \mathbb{C}^{N_r} whose dimension is $2N_r$. However, whenever we compare our reduced basis method with the ones constructed with real snapshots, we directly confront it with spaces that lie in \mathbb{R}^{N_r} rather than \mathbb{R}^{2N_r} . Having larger spaces reflects in a better accuracy; on the other side it increases the computational time. In our comparisons with real reduced spaces we have both these features.

2.4 Sensitivity of reduced basis methods

The solution of a discrete problem is always affected by the finite arithmetic precision of the linear solver. The construction of the reduced space starts from the solution of full problems, however this

process is affected by errors and therefore one should control that the resulting reduced space (and thus the perturbed reduced problem) still guarantees a reliable approximation of the full problem. Given an integration contour and given a set of quadrature points we adopt the following notation:

$$A_j(\mu) = z_j I - A(\mu), \quad f_j(\mu) = u_0 + \hat{b}(z_j; \mu), \quad x_j(\mu) = A_j^{-1} f_j(\mu), \quad \tilde{x}_j = A_j^{-1} \tilde{f}_j(\mu);$$

where $\tilde{f}_j(\mu)$ is a perturbation of $f_j(\mu)$.

We construct the matrix \tilde{B} of dimension N_r , which identify the reduced space, collecting snapshots of the perturbed full problems

$$A_j(\mu) \tilde{x}_j = \tilde{f}_j(\mu), \quad \forall j = 1, \dots, N-1, \quad \text{for some } \mu \in \mathcal{D};$$

we then have the perturbed reduced systems

$$\tilde{B}^H A_j(\mu) \tilde{x}_j^r(\mu) = \tilde{B}^H \tilde{f}_j(\mu), \quad \forall j = 1, \dots, N-1.$$

We define the perturbed solution manifold as

$$\tilde{\mathcal{M}}_h := \left\{ \tilde{x}_j(\mu) \mid \mu \in \mathcal{D}, j \in \{1, \dots, N-1\} \right\} \subset \mathbb{C}^{N_h},$$

and the associated Kolmogorov n -width

$$d_n(\tilde{\mathcal{M}}_h) := \inf_{\dim(Y)=n} \sup_{\tilde{x} \in \tilde{\mathcal{M}}_h} \text{dist}(\tilde{x}, Y).$$

The next Proposition 1 estimates from above the error

$$e(t, \mu) = \|u(t, \mu) - \tilde{u}_r(t, \mu)\|,$$

where $u(t, \mu)$ is given by (7) and $\tilde{u}_r(t, \mu)$ is given by

$$\tilde{u}_r(t, \mu) = \frac{c}{iN} \sum_{j=1}^{N-1} e^{z_j t} \tilde{x}_j^r(\mu) z_j', \quad \text{with } j = 1, \dots, N-1.$$

Proposition 1. For any $\mu \in \mathcal{D}$, $t \in \mathbb{R}^+$ and $N_r \in \mathbb{N}$ it holds

$$e(t, \mu) \leq \frac{c}{N} \sum_{j=1}^{N-1} \left(e^{\text{Re}(z_j)t} |z_j'| \left(\omega_j(\mu) + \left(1 + \frac{\gamma_j(\mu)}{\alpha_j(\mu)} \right) \left(\sup_{\mu \in \mathcal{D}} \max_{1 \leq j \leq N-1} \omega_j(\mu) + d_{N_r}(\mathcal{M}_h) \right) \right) \right);$$

where

$$\omega_j(\mu) = \left\| A_j^{-1}(\mu) \right\| \left\| f_j(\mu) - \tilde{f}_j(\mu) \right\|.$$

Proof.

$$\begin{aligned}
e(t, \mu) &= \|u(t, \mu) - \tilde{u}_r(t, \mu)\| \leq \frac{c}{N} \sum_{j=1}^{N-1} \left(e^{\operatorname{Re}(z_j)t} |z'_j| \|x_j(\mu) - \tilde{x}_{rj}(\mu)\| \right) \\
&\leq \frac{c}{N} \sum_{j=1}^{N-1} \left(e^{\operatorname{Re}(z_j)t} |z'_j| \left(\|x_j(\mu) - \tilde{x}_j(\mu)\| + \|\tilde{x}_j(\mu) - \tilde{x}_{rj}(\mu)\| \right) \right) \\
&\leq \frac{c}{N} \sum_{j=1}^{N-1} \left(e^{\operatorname{Re}(z_j)t} |z'_j| \left(\omega_j(\mu) + \left(\left(1 + \frac{\gamma_j(\mu)}{\alpha_j(\mu)} \right) \inf_{v \in \operatorname{Im}(\tilde{B})} \|\tilde{x}_j(\mu) - v\| \right) \right) \right) \\
&\leq \frac{c}{N} \sum_{j=1}^{N-1} \left(e^{\operatorname{Re}(z_j)t} |z'_j| \left(\omega_j(\mu) + \left(\left(1 + \frac{\gamma_j(\mu)}{\alpha_j(\mu)} \right) d_{N_r}(\tilde{\mathcal{M}}_h) \right) \right) \right),
\end{aligned}$$

where we recall that \tilde{B} is the matrix identifying the reduced space generated from the perturbed problem. To get to the last expression we first used the triangular inequality and then the Céa's Lemma for the perturbed problem. We now need to bound the N -width of the perturbed problem. We have

$$\begin{aligned}
d_{N_r}(\tilde{\mathcal{M}}_h) &= \inf_{\dim(Y)=N_r} \sup_{\tilde{x} \in \tilde{\mathcal{M}}_h} \inf_{v \in Y} \|\tilde{x} - v\| \\
&\leq \inf_{\dim(Y)=N_r} \sup_{\tilde{x} \in \tilde{\mathcal{M}}_h} \inf_{v \in Y} \|\tilde{x} - x + x - v\| \\
&\leq \inf_{\dim(Y)=N_r} \sup_{\tilde{x} \in \tilde{\mathcal{M}}_h} \inf_{v \in Y} (\|\tilde{x} - x\| + \|x - v\|) \\
&\leq \sup_{\tilde{x} \in \tilde{\mathcal{M}}_h} \|\tilde{x} - x\| + d_{N_r}(\mathcal{M}_h) \\
&\leq \sup_{\mu \in \mathcal{D}} \max_{1 \leq j \leq N-1} \left\| A_j^{-1}(\mu) \right\| \left\| f_j(\mu) - \tilde{f}_j(\mu) \right\| + d_{N_r}(\mathcal{M}_h). \tag{17}
\end{aligned}$$

□

As a consequence, up to

$$\sup_{\mu \in \mathcal{D}} \max_{1 \leq j \leq N-1} \left\| A_j^{-1}(\mu) \right\| \left\| f_j(\mu) - \tilde{f}_j(\mu) \right\|,$$

the decay of $d_{N_r}(\tilde{\mathcal{M}})$ with respect to N_r is at least as fast as the one of $d_{N_r}(\mathcal{M})$.

Proposition 1 states that the error between the solution of the full problem and the solution of the perturbed reduced problem depends on two factors: the resolvent norm, which we control in the construction of the integration profile, and the Kolmogorov N -width associated to the full problem, which we assume to know a priori.

2.5 Offline-Online phases

According to the literature, the offline phase is the stage where the reduced space is constructed. This phase is the one computationally demanding since building the reduced space requires the

solution of several full problems as we are going to see in the next section. The online phase is the one where the reduced solution $u_r(t; \mu)$, (see (16)), is computed. In an ideal setting, the cost of accomplishing this should be independent of the complexity of the full problem, which depends on N_h , and should depend only on the size N_r of the reduced basis approximation. To compute $u_r(t; \mu)$ we need to solve (14), that is

$$\beta_j = (z_j I_{N_r} - A_r(\mu))^{-1} (u_{0r} + \hat{b}_r(z_j; \mu)), \quad \text{for } j = 1, \dots, N - 1,$$

being I_{N_r} the $N_r \times N_r$ identity matrix,

$$A_r(\mu) = B^H A(\mu) B, \quad (18)$$

$$\hat{b}_r(z_j; \mu) = B^H \hat{b}(z_j; \mu), \quad (19)$$

$$u_{0r} = B^H u_0. \quad (20)$$

with B the $N_h \times N_r$ matrix whose columns coincide with the reduced space basis functions ζ_j , $j = 1, \dots, N_r$. This requires to form (18) and (19) for each instance of μ whose cost still depends on N_h (since $A(\mu) \in \mathbb{R}^{N_h \times N_h}$, $B \in \mathbb{C}^{N_h \times N_r}$ and $\hat{b}(z; \mu) \in \mathbb{C}^{N_h}$). However, this can be done by assuming that the forms $A(\mu)$ and $\hat{b}(z; \mu)$ admit the affine decomposition

$$A(\mu) = \sum_{q=1}^{Q_A} \Theta_A^q(\mu) A^q \quad \forall \mu \in \mathcal{D}, \quad (21)$$

$$\hat{b}(z, \mu) = \sum_{q=1}^{\hat{Q}_b} \Theta_b^q(\mu) \hat{b}^q(z) \quad \forall \mu \in \mathcal{D}; \quad (22)$$

where each operator

$$A^q \in \mathbb{R}^{N_h \times N_h}, \quad \hat{b}^q(z) \in \mathbb{C}^{N_h},$$

is independent from the parameter μ and the coefficients $\Theta_A^q : \mathcal{D} \rightarrow \mathbb{R}$, $\Theta_b^q : \mathcal{D} \rightarrow \mathbb{R}$ are scalar. Therefore Q_A square matrices of dimension N_r , say A_r^q (each associated to A^q), can be precomputed in the offline phase once the reduced basis space is known. This computation is done only once and in parallel since the A^q matrices are independent from μ . Then, during the online stage, when a new instance of the parameter μ is introduced, the new solution matrix is built as

$$A_r(\mu) = \sum_{q=1}^{Q_A} \Theta_A^q(\mu) A_r^q.$$

This operation is independent of N_h and scales proportionally to $Q_A \cdot N_r$. The treatment of the linear forms $\hat{b}(z, \mu)$ is analogous.

For cases where an affine decomposition is not available, one can often find an approximate form that satisfies this property through empirical interpolation (see e.g. [1]) or empirical cubature methods (see e.g. [8, 31, 24]). However, for the propose of this work, we assume the affine decomposition is available.

3 Reduced basis space generation

As two of the most employed strategies to generate reduced spaces we consider the proper orthogonal decomposition (POD) [28] and the greedy algorithm [27]. These two are also combined when dealing with time dependent problems.

In this section we introduce an error estimator based on our discrete problem formulation, then we use it to define two novel greedy algorithms which provide suitable reduced basis to solve the time integration with contour integral methods.

3.1 Greedy basis generation

The standard greedy generation of the reduced space is an iterative procedure where at each iteration one new basis function is added and the overall approximation capability of the basis set is improved. It requires one high fidelity solution to be computed per iteration and a total of N_r truth solutions to generate the N_r -dimensional reduced basis space. An essential ingredient of the greedy algorithm is the availability of an error estimate $\Delta(\mu)$ which predicts the error due to the model order reduction. It provides an estimate of the error induced by replacing the full space of dimension N_h by the reduced basis space of dimension N_r . Such approach is also denoted as weak-greedy algorithm, to distinguish it from the strong-greedy algorithm where the direct measure of the error is employed. A strong-greedy algorithm requires the evaluation of the high fidelity solution for each instance of the parameters in the parametric domain, which is against the principle of model order reduction. For this reason the error estimator $\Delta(\mu)$ should be computationally cheap to evaluate for every $\mu \in \mathcal{D}$. A key feature of this strategy is the ability to construct subspaces which preserve the type of decay of the Kolmogorov n -width inherited by the underlying problem. The results in [2] ensure that the convergence rate of the weak greedy approach does not change. Let us define the residual at the point z_j as the vector generated by replacing $\hat{u}(z_j; \mu)$ with $\hat{u}_r(z_j; \mu)$ into (3), i.e.

$$r(z_j; \mu) = \left(z_j I - A(\mu) \right) \hat{u}_r(z_j; \mu) - u_0(\mu) - \hat{b}(z_j; \mu),$$

so that

$$\hat{u}_r(z_j; \mu) = \left(z_j I - A(\mu) \right)^{-1} \left(r(z_j; \mu) + u_0(\mu) + \hat{b}(z_j; \mu) \right). \quad (23)$$

Proposition 2. For a prescribed time window $[t_0, t_1] \subset \mathbb{R}^+$ and for all $\mu \in \mathcal{D}$ it holds that

$$\max_{t \in [t_0, t_1]} \left\| u(t, \mu) - u_r(t, \mu) \right\| \leq \Delta(\mu),$$

where the error estimator $\Delta(\mu)$ is given by

$$\Delta(\mu) := \max_{t \in [t_0, t_1]} \left(\frac{c}{N} \sum_{j=1}^{N-1} e^{\operatorname{Re}(z_j)t} \left| z'_j \right| \left\| \left(z_j I - A(\mu) \right)^{-1} \right\| \left\| \hat{r}(z_j; \mu) \right\| \right). \quad (24)$$

Proof. We have

$$\begin{aligned}
\max_{t \in [t_0, t_1]} \|u(t, \mu) - u_r(t, \mu)\| &= \max_{t \in [t_0, t_1]} \left(\frac{c}{N} \left\| \sum_{j=1}^{N-1} e^{z_j t} z_j' (\hat{u}(z_j; \mu) - \hat{u}_r(z_j; \mu)) \right\| \right) \\
&\leq \max_{t \in [t_0, t_1]} \left(\frac{c}{N} \sum_{j=1}^{N-1} e^{\operatorname{Re}(z_j) t} |z_j'| \left\| \hat{u}(z_j; \mu) - \hat{u}_r(z_j; \mu) \right\| \right) \\
&\leq \max_{t \in [t_0, t_1]} \left(\frac{c}{N} \sum_{j=1}^{N-1} e^{\operatorname{Re}(z_j) t} |z_j'| \left\| (z_j I - A(\mu))^{-1} \right\| \left\| \hat{r}(z_j; \mu) \right\| \right) \\
&= \Delta(\mu),
\end{aligned} \tag{25}$$

where we have made use of (16), (3) and (23). \square

As mentioned, a good error estimator needs to be cheaply computed for all $\mu \in \mathcal{D}$. The maximum over the time window is fast to compute since the dependence from t only appears in the scalar exponential term. The dependence of $\Delta(\mu)$ on μ is in the norm of the residual and in the norm of the resolvent. The first one is easy to evaluate for each value of μ (see [14, Section 4.2.5]). The second one involves the computation of the smallest singular value of $z_j I - A(\mu)$ whose evaluation $\forall \mu \in \mathcal{D}$ is computationally expensive. Therefore the strategy employed is to look for an upper bound for $\|(z_j I - A(\mu))^{-1}\|$ which has to be cheap to compute. Note that the integration contour is constructed in such a way that $\|(z_j I - A(\mu))^{-1}\|$ is bounded, however the use of this bound in (24) is far from being sharp. In Section 3.4 we shall review the methods proposed in literature to deal with this problem and we will describe a new approach based on a suitable optimization procedure.

Finally, in order to characterize the sharpness of the error estimate, we introduce the effectivity index:

$$\mathbf{eff}(\mu) = \frac{\Delta(\mu)}{e\hat{r}r(\mu)},$$

where $e\hat{r}r$ is defined as

$$e\hat{r}r(\mu) := \max_{t \in [t_0, t_1]} \left(\frac{c}{N} \sum_{j=1}^{N-1} e^{\operatorname{Re}(z_j) z_j t} |z_j'| \left\| \hat{u}(z_j; \mu) - \hat{u}_r(z_j; \mu) \right\| \right).$$

Proposition 3. For $\mu \in \mathcal{D}$ we have

$$\mathbf{eff}(\mu) \leq \max_{1 \leq j \leq N-1} \left[\left\| (z_j I - A(\mu))^{-1} \right\| \right] \cdot \max_{1 \leq j \leq N-1} \left[\left\| (z_j I - A(\mu)) \right\| \right].$$

Proof. We note that

$$\begin{aligned}
\text{eff}(\mu) &\leq \frac{\max_{t \in [t_0, t_1]} \left(\sum_{j=1}^{N-1} e^{\text{Re}(z_j)z_j t} |z'_j| \left\| (z_j I - A(\mu))^{-1} \right\| \left\| \hat{r}(z_j; \mu) \right\| \right)}{\max_{t \in [t_0, t_1]} \left(\sum_{j=1}^{N-1} e^{\text{Re}(z_j)z_j t} |z'_j| \left\| \hat{u}(z_j; \mu) - \hat{u}_r(z_j; \mu) \right\| \right)} \\
&\leq \frac{\max_{t \in [t_0, t_1]} \left(\sum_{j=1}^{N-1} e^{\text{Re}(z_j)z_j t} |z'_j| \left\| (z_j I - A(\mu))^{-1} \right\| \left\| \hat{r}(z_j; \mu) \right\| \right)}{\max_{t \in [t_0, t_1]} \left(\sum_{j=1}^{N-1} e^{\text{Re}(z_j)z_j t} |z'_j| \left\| (z_j I - A(\mu)) \right\|^{-1} \left\| \hat{r}(z_j; \mu) \right\| \right)} \\
&\leq \frac{\max_j \left\| (z_j I - A(\mu))^{-1} \right\|}{\min_j \left\| (z_j I - A(\mu)) \right\|^{-1}} \\
&= \max_{j \in \{1, \dots, N-1\}} \left[\left\| (z_j I - A(\mu))^{-1} \right\| \right] \cdot \max_{j \in \{1, \dots, N-1\}} \left[\left\| (z_j I - A(\mu)) \right\| \right].
\end{aligned}$$

□

3.2 The inverse Laplace transform Greedy-POD algorithm

A widely used sampling strategy to construct reduced basis spaces for the time dependent problem is based on the combined use of POD in time with greedy sampling in the parameter space \mathcal{D}_δ where \mathcal{D}_δ is a finite subset of \mathcal{D} . It can consist of a regular lattice or a randomly generated point-set intersecting with \mathcal{D} . The fact that such strategy is able to construct reduced spaces which preserve the exponential or algebraic convergence rates of the Kolmogorov n -width is shown in [13].

Our approach consists of replacing the proper orthogonal decomposition in time with the one in the Laplace transform domain. The steps for the construction of the reduced basis are reported in Algorithm 1. At each iteration, for the selected vector of parameters μ_m , the algorithm first computes the Laplace transform of the solution on the quadrature nodes, then it compresses the collected snapshots, up to the prescribed tolerance tol_{POD} , and finally it computes the vector of parameters which maximize the error estimator. It stops when the error estimator is smaller then the prescribed accuracy tol for each value of $\mu \in \mathcal{D}_\delta$.

3.3 An alternative approach: local reduced basis on the quadrature nodes

Once a parameter is selected, Algorithm 1 computes the high fidelity solution related to that parameter on each quadrature nodes and it adds those solutions to the reduced space. Therefore, the constructed reduced space turns out to be an approximation of the whole solution manifold (13). Another strategy consists of approximating the solutions manifold associated to each quadrature node, i.e. to consider

$$\mathcal{M}_h^j = \{\hat{u}(z_j; \mu) \mid \mu \in \mathcal{D}_\delta\}, \quad j = 1, \dots, N-1;$$

Algorithm 1 POD-Greedy construction of the reduced space

Input: $tol, tol_{POD}, \mu_1, m = 1, \mathbb{B} = \emptyset$
Output: The reduced space: $\mathbb{V}_r = \text{span}\{\zeta_1, \dots, \zeta_{N_r}\}$

- 1: **while** $\Delta(\mu_m) > tol$ **do**
- 2: **for** $j = 1, \dots, N - 1$ **do**
- 3: Compute $\hat{u}(z_j; \mu_m) = (z_j I - A(\mu_m))^{-1}(u_0 + \hat{b}(z; \mu_m))$, $z_j = z(\xi_j)$
- 4: **end for**
- 5: $\mathbb{B} = \{\mathbb{B}, \{\hat{u}(z_1; \mu_m), \dots, \hat{u}(z_{N-1}; \mu_m)\}\}$
- 6: Compute $[\zeta_1, \dots, \zeta_{N_r}] = \text{POD}(\mathbb{B}, tol_{POD})$
- 7: Set $\mathbb{V}_r = \{\zeta_1, \dots, \zeta_{N_r}\}$
- 8: Compute $\mu_{m+1} = \arg \max_{\mu \in \mathcal{D}_\delta} \Delta(\mu)$
- 9: Set $m = m + 1$
- 10: **end while**

Algorithm 2 Greedy construction of the reduced space at the j -th quadrature node

Input: tol, μ_1, j
Output: The reduced space: \mathbb{V}_r^j

- 1: Set $\mathbb{B} = []$, $m = 1$, $\Delta_j(\mu) = \frac{c}{N} \max_{t \in [t_0, t_1]} (e^{\text{Re}(z_j)t}) \left\| z'_j \left\| (z_j I - A(\mu))^{-1} \right\| \left\| \hat{r}(z_j; \mu) \right\| \right\|$
- 2: **while** $\Delta_j(\mu_m) > \left(\frac{tol}{N-1}\right)$ **do**
- 3: Compute $\hat{u}(z_j; \mu_m) = (z_j I - A(\mu_m))^{-1}(u_0 + \hat{b}(z; \mu_m))$, $z_j = z(\xi_j)$
- 4: $\mathbb{B} = \{\mathbb{B}, \hat{u}(z_j; \mu_m)\}$
- 5: $\mathbb{V}_r^j = \text{orth}\{\mathbb{B}\}$
- 6: Compute $\mu_{m+1} = \arg \max_{\mu \in \mathcal{D}_\delta} \Delta_j(\mu)$
- 7: $m = m + 1$
- 8: **end while**

and approximating separately each of these solutions sets.

Since we are interested in the solution $u(t, \mu)$ we still rely on the error estimate (24), but this time the stopping criteria for the greedy algorithm is that each term of the sum in (24) is required to be smaller than the given tolerance divided by $N - 1$. The strategy is summarized in Algorithm 2.

In general, the reduced spaces constructed at each quadrature point by Algorithm 2 are of different sizes. Indeed, due to the presence of the exponential term $e^{\text{Re}(z_j)t}$ in Δ_j , the size of the spaces is expected to be larger for those nodes with positive real part and smaller for the nodes with large and negative real part.

The main difference between Algorithm 1 and Algorithm 2, is that the first collects all the basis vectors together and then it constructs a unique reduced space, while the second one builds a specific reduced space for each quadrature node. As a result, the size of the reduced space in the first approach turns out to be larger than any of the sets constructed with the second one.

From a computational point of view, we require a greedy type search with Algorithm 2 on each quadrature point while Algorithm 1 has only one greedy type search. For a fixed accuracy tol , since the dimension of the local reduced spaces is smaller than the dimension of the space constructed with Algorithm 1, the computation of $\Delta(\mu) \forall \mu \in \mathcal{D}_\delta$ is faster with the local approach, but it needs

to be performed at each quadrature point. Note that the construction of the reduced basis on the quadrature nodes in Algorithm 2 can be parallelized in a natural way.

From a storage point of view the cost is higher for Algorithm 2 since, in Algorithm 1, redundant information across the nodes are compressed thanks to the POD.

We will discuss the computational and storage costs associated to the two algorithms in Section 4, which is dedicated to numerical experiments.

3.4 The resolvent norm

The error estimate (24) depends on the resolvent norm. It holds that

$$\|(zI - A(\mu))^{-1}\| = \frac{1}{\sigma_{min}(\mu)},$$

where $\sigma_{min}(\mu)$ is the smallest singular value of $zI - A(\mu)$. The direct computation of $\sigma_{min}(\mu)$ $\forall \mu \in \mathcal{D}_\delta$ is an expensive procedure that one aims to avoid in the framework of reduced basis method. Few techniques have been developed to perform a fast and cheap estimation of $\sigma_{min}(\mu)$; in particular we mention the Successive Constrain Minimization method (SCM) [20, 4, 15] and the heuristic strategy based on radial basis functions interpolation (RBF) [25].

The SCM is an offline/online procedure in which generalized eigenvalue problems of size N_h need to be solved during the offline phase. The online part is then restricted to provide a lower bound $\tilde{\sigma}_{LB}(\mu)$ of the smallest singular value $\sigma_{min}(\mu)$ for each new parameter $\mu \in \mathcal{D}_\delta$ with an operation complexity that is independent of the dimension N_h . Nevertheless, although this procedure enables a very rapid online evaluation of the stability factor, it still requires a quite expensive offline stage (see numerical experiments of Section 4), which may jeopardize the efficiency of the whole reduction process.

The heuristic strategy proposed in [25] combines a radial basis interpolant to the smallest singular value, incorporating suitable criteria to ensure its positivity, with an adaptive choice of interpolation points through a greedy procedure. In this way it is possible to obtain a reliable approximation of $\sigma_{min}(\mu)$, whose offline construction and online evaluation are fast. This strategy turns out to be effective in our applications but it lacks rigorous theoretical foundations. In fact, for multivariate interpolation the error introduced by the approximation is not quantifiable as in the one-dimensional case.

We propose instead a simple approach based on the computation of the lower bound

$$\tilde{\sigma}_{LB} = \inf_{\mu \in \mathcal{D}} \sigma_{min}(\mu). \quad (26)$$

The optimization is performed by a gradient-descent iteration method, i.e. given the parameter μ_i at iteration i we compute the update at iteration $i + 1$ as

$$\mu_{i+1} = \mu_i - \delta_i \nabla \sigma_{min}(\mu_i) \quad i \geq 0$$

where μ_0 is suitably chosen and δ_i is a variable step size. Since the optimization problem (26) is not convex, this method converges to a local minimum, therefore to be effective one should have some knowledge about the behaviour of $\sigma_{min}(\mu)$ with respect to the parameters and should combine the

local optimization with a globalization strategy. For instance one could set different starting point μ_0 or may partition \mathcal{D} into several sub-domains \mathcal{D}_j such that $\mathcal{D} = \bigcup_{j=1}^J \mathcal{D}_j$ and then minimize $\sigma_{min}(\mu)$ on each sub-domain. The expression of the partial derivatives associated to $\nabla \sigma_{min}(\mu)$ can be computed analytically. In fact we have for a simple non zero singular value (see e.g. [23, 17]),

$$\frac{\partial \sigma_{min}(\mu)}{\partial \mu_i} = \text{Re} \left(\hat{u}^* \left(\frac{\partial A(\mu)}{\partial \mu_i} \right) \hat{v} \right) \quad \text{for } i = 1, \dots, d;$$

where \hat{u} and \hat{v} are the associated left and right singular vectors, respectively, to $\sigma_{min}(\mu)$. See [12, Section 3] for more details. Due to assumption (21) the expression of $\frac{\partial A}{\partial \mu_i}$ simply reduces to

$$\frac{\partial A(\mu)}{\partial \mu_i} = \sum_{q=1}^{Q_A} \frac{\partial \Theta_A^q(\mu)}{\partial \mu_i} A^q \quad \text{for } i = 1, \dots, d.$$

An advantage of the optimization is that we do not need to prescribe a discrete counterpart of \mathcal{D} , while for SCM and interpolation, we are forced to use a discrete set as training sample. To enforce the procedure we choose different starting points μ_0 , for example the vertexes of \mathcal{D} .

3.5 Choice of the integration profile

The integration profile is chosen according to the information provided by the approximation of the weighted ϵ -pseudospectrum of $A(\mu)$ (see [11]). The set is crucial in order to control the numerical error due to the fact that we operate in finite precision arithmetic. This quantity was estimated in [12] as

$$err_N^{num} \leq \frac{c}{N} \sum_{j=1}^{N-1} e^{\text{Re}(z(x_j))t} \|(z_j \mathbf{I} - A(\mu))^{-1}\| \|r_j(\mu)\| |z'(x_j)|;$$

where $r_j(\mu)$ is the residual originated by the numerical solution of $(z_j \mathbf{I} - A(\mu))\hat{u} = u_0 + \hat{b}(z_j; \mu)$. Therefore, in order to construct a unique integration profile, one needs information about the ϵ -pseudospectrum of $A(\mu)$ for each $\mu \in \mathcal{D}_\delta$. The approximation of weighted ϵ -pseudospectrum level sets is computationally onerous and despite new methods have been recently proposed to reduce the cost of the approximation procedure (see [12]), it is not feasible to compute this set for each $\mu \in \mathcal{D}$. To overcome this problem we adopted the following strategy:

1. we fix a reference parameter $\mu^* \in \mathcal{D}_\delta$ and we construct the integration contour related to the operator $A(\mu^*)$;
2. for each quadrature node z_i we compute

$$\tilde{\sigma}_{LB}^i = \min_{\mu \in \mathcal{D}_\delta} \sigma_{min}^i(\mu), \quad \mu^i = \arg \min_{\mu \in \mathcal{D}_\delta} \sigma_{min}^i(\mu),$$

according the procedure described in Section 3.4;

3. for each μ^i and for $t \in [t_0, t_1]$ we estimate err_N^{num} as

$$\begin{aligned} err_N^{num} &\leq \frac{c}{N} \sum_{j=1}^{N-1} e^{\operatorname{Re}(z(x_j))t} \|(z_j \mathbf{I} - A(\mu^i))^{-1}\| \|r_j(\mu^i)\| |z'(x_j)| \\ &\leq \frac{c}{N} \sum_{j=1}^{N-1} e^{\operatorname{Re}(z(x_i))t} \frac{1}{\tilde{\sigma}_{LB}^j} \|r_j(\mu^i)\| |z'(x_j)|; \end{aligned} \quad (27)$$

4. if (27) is smaller than the prescribed tolerance for each i we confirm our initial guess as integration profile, otherwise we construct the integration profile related to one of the $A(\mu^i)$ for which (27) is too large and we iterate steps 1-2-3 until a suitable integration profile is determined.

This procedure turns out to be effective in all our test problems.

4 Numerical tests

In this section we show few numerical results to validate our method. We first test our approach with the Black–Scholes and Heston equations. The Black–Scholes model here is the same as the one considered in [19], while for the Heston model we consider a slightly different boundary condition from that in [19], following [18]. Then we consider a canonical advection equation, which we already mentioned to be challenging for reduced basis methods based on time step discretization.

With this test problems we aim to demonstrate the effectivity of our methodology; moreover we show that our approach does not suffer of a large size reduced basis when dealing with linear hyperbolic problems and, in general, when a convection term is present. We refer to the reduction associated to the time step discretization as classical reduced basis or classical reduction while we call Laplace reduced basis the strategy we have presented in the previous sections. Regarding the classical reduction strategy, for the Black-Scholes test problem we constructed the classical reduced spaces with the greedy-POD algorithm while, for the Heston and advection test problem cases we used POD to compress the information acquired through computation of the full order solutions on each time step and on a prescribed train parameter sample. All the computations were performed using `Matlab 2021a` on a laptop with 2.60 GHz Intel Core i7 processor.

4.1 Black–Scholes equation

The well known (deterministic) Black-Scholes equation (see e.g. [3]) has the following form:

$$\frac{\partial u}{\partial \tau} = \frac{1}{2} \sigma^2 s^2 \frac{\partial^2 u}{\partial s^2} + r s \frac{\partial u}{\partial s} - r u, \quad s > L, \quad 0 < \tau \leq t, \quad (28)$$

for L, t given, where the unknown function $u(s, \tau)$ stands for the fair price of the option when the corresponding asset price at time $t - \tau$ is s , and t is the maturity time of the option. Moreover,

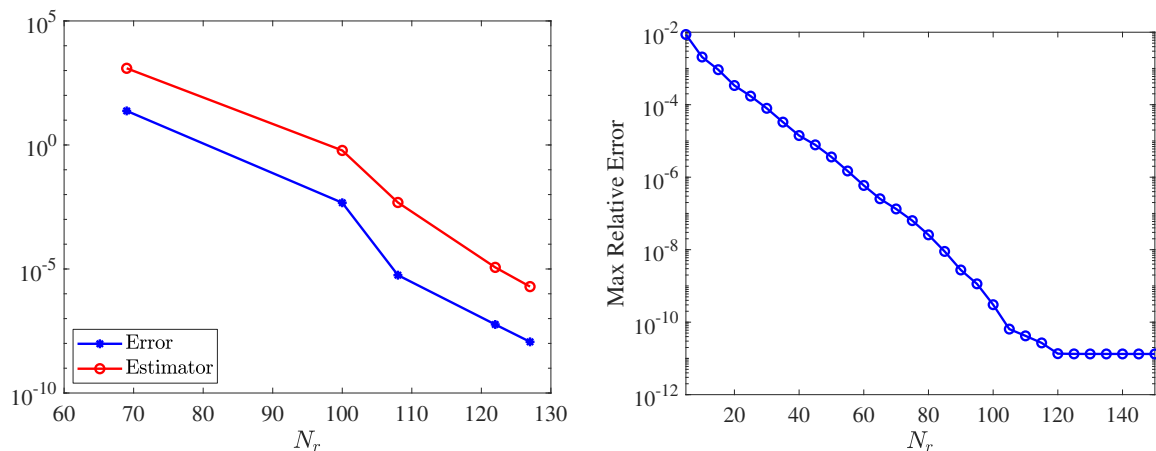


Figure 1: Black-Scholes test problem. Behaviour of the Greedy-POD selection algorithm (left); decay of the relative error (30) with respect to the reduced basis size (right).

$r \geq 0$, $\sigma > 0$ are given constants (representing the interest rate and the volatility, respectively). In practice we consider a bounded spatial domain, setting

$$L < s < S$$

for a sufficiently large S . We study (28) with the following conditions, typical of the European option call, (see [21]):

$$\begin{aligned} u(s, 0) &= \max(0, s - K), \\ u(L, \tau) &= 0, \quad 0 \leq \tau \leq t, \\ u(S, \tau) &= S - e^{-r\tau}K, \quad 0 \leq \tau \leq t, \end{aligned} \quad (29)$$

being K the reference strike price.

Following the same strategy adopted in [19], we discretize in space on a uniform grid of $n = 1000$ points in $[0, 200]$, using the classical centred finite difference scheme. We consider the time window $t \in [1, 10]$ and the parametric domain

$$\mu = [\sigma, r] \in \mathcal{D} = [0.05, 0.25] \times [0.001, 0.02],$$

which we restrict to the set Ξ made of 20×20 points uniformly distributed in \mathcal{D} . We measure the relative error as

$$E_r = \max_{\mu \in \Xi} \max_{t \in [1, 10]} \frac{\|u(t; \mu) - u_r(t; \mu)\|}{\|u(t; \mu)\|}. \quad (30)$$

Figure 1 shows the behaviour of Algorithm 1. Indeed, on the left picture, we see that the error estimator has the same behaviour of the absolute error as more parameter are selected to construct the reduced space, while, on the right plot, we recover the desired exponential decay of the relative error with respect to the size of the reduced basis.

Next we observe in Table 1 and Figure 2 the performances of Algorithm 1 and Algorithm 2. It turns out that Algorithm 2 is more expensive in terms of computational time and number of stored

	CPU time (s)	# Stored Snapshots
Algorithm 1	19	115
Algorithm 2	34	1143

Table 1: CPU time and number of stored snapshots with the greedy-POD strategy of Algorithm 1 and the local greedy strategy of Algorithm 2.

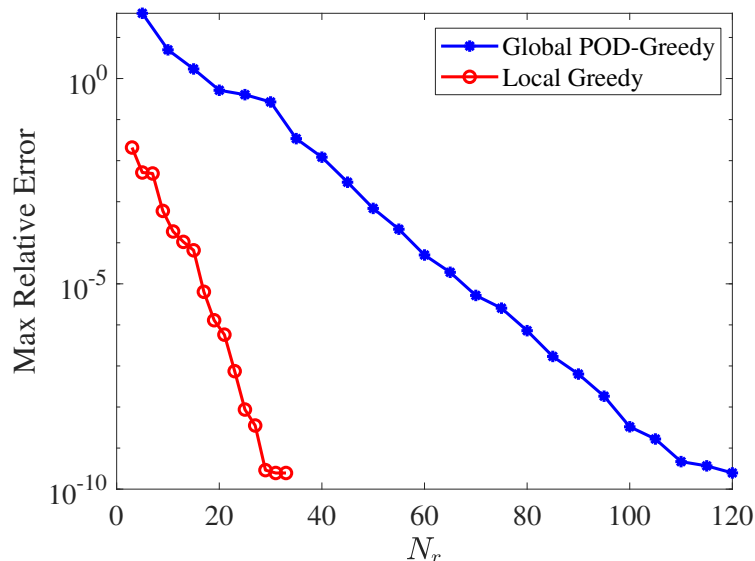


Figure 2: Black-Scholes test problem. Decay of the error (30), with respect to the reduced basis size constructed with the POD-Greedy strategy (Algorithm 1) and the local Greedy one (Algorithm 2). Time window $[1, 10]$ and $|\Xi| = 400$ uniformly distributed samples.

snapshots, while the decay of error with respect to the reduced basis size is clearly better. Based on these results we believe that Algorithm 2 is more suitable for this problem since the gain in the online phase is remarkable and the additional cost in the offline phase is modest (and may be reduced using multi core processors).

We have compared the Laplace reduced basis method with a classical one based on the Crank-Nicolson time scheme with constant stepsize $\Delta t = 10^{-4}$ on time window $[0.1, 1]$. The error in the full problem is around $5 \cdot 10^{-6}$ for Laplace and $1 \cdot 10^{-3}$ for Crank-Nicolson. Figure 3 displays the resolution times, averaged over the parametric domain Ξ , for the solution of the reduced problem. We note that the contour integral method is between the 8 and 18 times faster.

We also analysed the CPU time in the offline phase, i.e. the time needed to solve the full problem. In particular, we considered the Crank-Nicolson scheme with two time steps: $\Delta t = 10^{-4}$ and $\Delta t = 10^{-2}$; regarding the integration tolerance related to the contour integral method we have set the values $5 \cdot 10^{-6}$ and 10^{-2} . Results are displayed in Figure 4 where the CPU time is measured as an average of 100 different computations. When $\Delta t = 10^{-2}$, $tol = 10^{-2}$ and $T = 1$ (Figure 4(a) and Figure 4(b)) the CPU time is similar for the two solvers with the one related to the time step method being slightly lower. When we set the final time to $T = 10$ (Figure 4(c) and Figure 4(d))

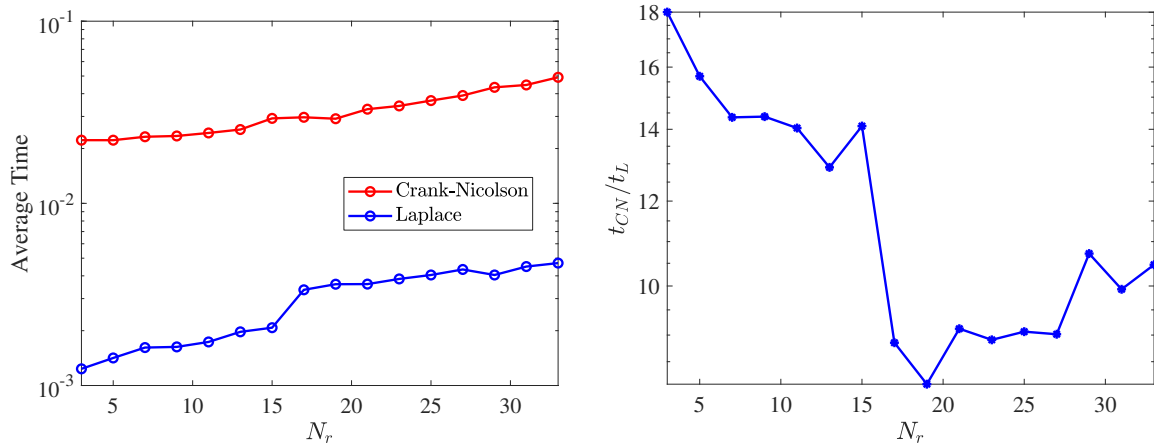
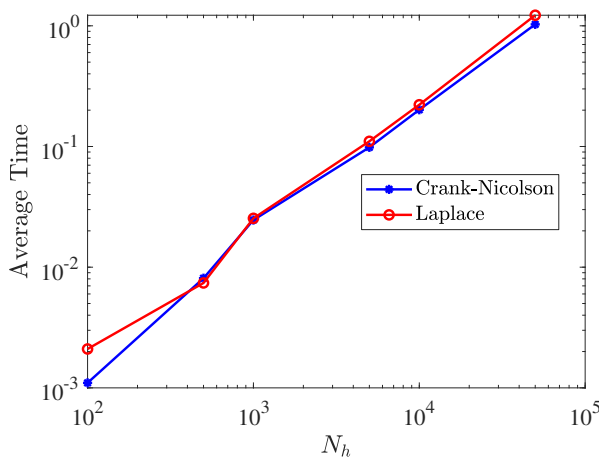


Figure 3: Black-Scholes test problem on the time window $[0.1, 1]$. Behaviour of the computational time with respect to size of the reduced basis for Crank-Nicolson and Laplace. Direct comparison (left) and ratio between the average times (right).

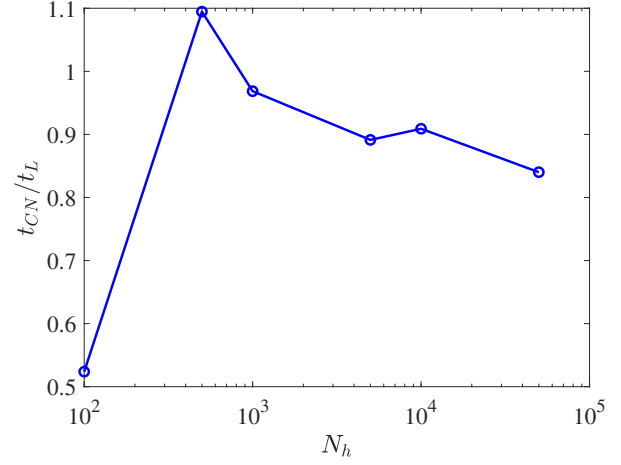
we do not see relevant changes in the CPU time of the Laplace method, while the one of Crank-Nicolson clearly increases making it slower than the contour integral method. Also, considering the time window $[0.1, 1]$ and increasing the time accuracy, the contour integral method outperforms the time step scheme being between the 7 and 14 times faster (see Figure 4(f)).

Figure 5 displays two plots which compare the two reduction techniques. The left one concerns the behaviour of the maximum relative error with respect to size of the reduced basis, the error originated by the Laplace reduced basis is always below the one associated to the classical reduced basis method, being also significantly smaller for most of the values of N_r . Concerning the classical method we have an initial stagnation which precedes a rapid decrease of the error. This feature may be explained by the presence of convection, which cannot be neglected. Also, the initial datum is only continuum a feature, which, combined with convection can originate a slow decay of the reduction error for classical reduced basis methods. The right plot compares the two reduction techniques in terms of computational time with respect to the reduction error. It can be seen that the Laplace reduced basis is almost two order of magnitude faster than the classical reduced basis method.

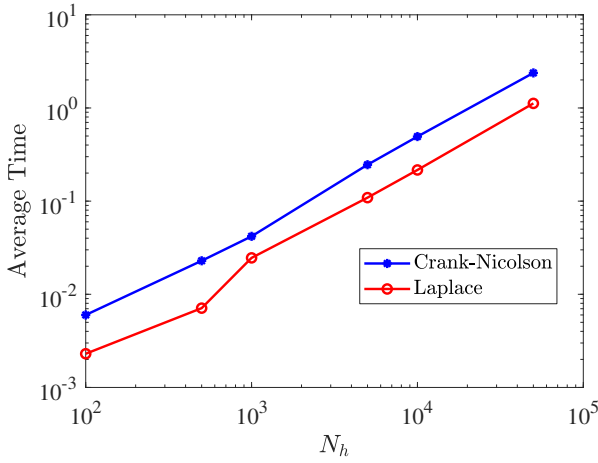
Finally we illustrate the results obtained through the gradient based strategy for the computation of $\tilde{\sigma}_{LB}$, see (26). As first result we show that the Black-Scholes problem is well suited to be treated with a gradient type method. Figure 6 shows the computed smallest singular value for each parameter in Ξ and for 2 quadrature points. We found that the shape of the second plot is assumed in most of the quadrature points. It can be seen that the smallest singular value is quite smooth with respect to the parameters in all the cases considered. In Table 3 we report the computed approximation for $\tilde{\sigma}_{LB}$, denoted as $\tilde{\sigma}_{GS}$, for 10 quadrature points together with the relative error and the number of eigenvalue problems solved to provide the final approximation. We set four starting points according to the criteria described in Section 3.4. With a maximum of 22 eigenvalues computations the method is able to return the exact lower bound on the parametric



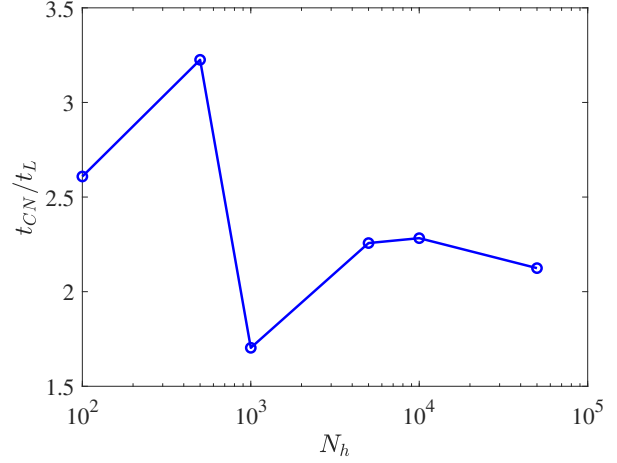
(a) $\Delta t = 10^{-2}$, $tol = 10^{-2}$, $t \in [0.1, 1]$



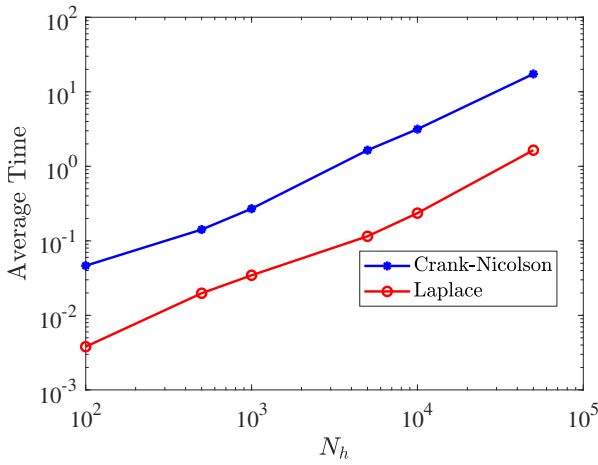
(b) $\Delta t = 10^{-2}$, $tol = 10^{-2}$, $t \in [0.1, 1]$



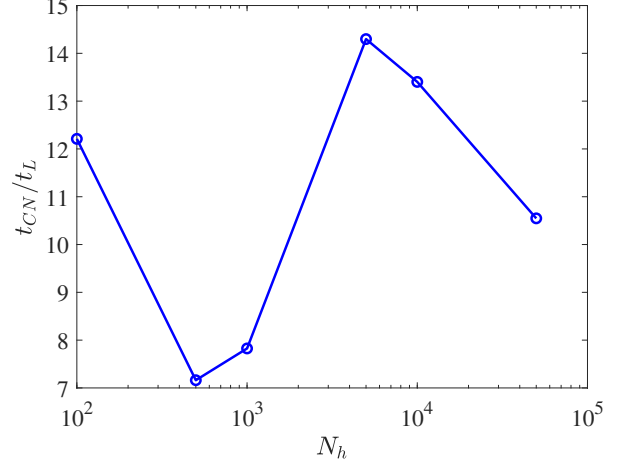
(c) $\Delta t = 10^{-2}$, $tol = 10^{-2}$, $t \in [1, 10]$



(d) $\Delta t = 10^{-2}$, $tol = 10^{-2}$, $t \in [1, 10]$



(e) $\Delta t = 10^{-4}$, $tol = 5 \cdot 10^{-6}$, $t \in [0.1, 1]$



(f) $\Delta t = 10^{-4}$, $tol = 5 \cdot 10^{-6}$, $t \in [0.1, 1]$

Figure 4: Black-Scholes equation for different choices of Δt , tol and time window. On the left: averaged CPU time with respect to the discretization size N_h for Crank-Nicolson and Laplace. On the right: ratio between the CPU time of Crank-Nicolson and Laplace.

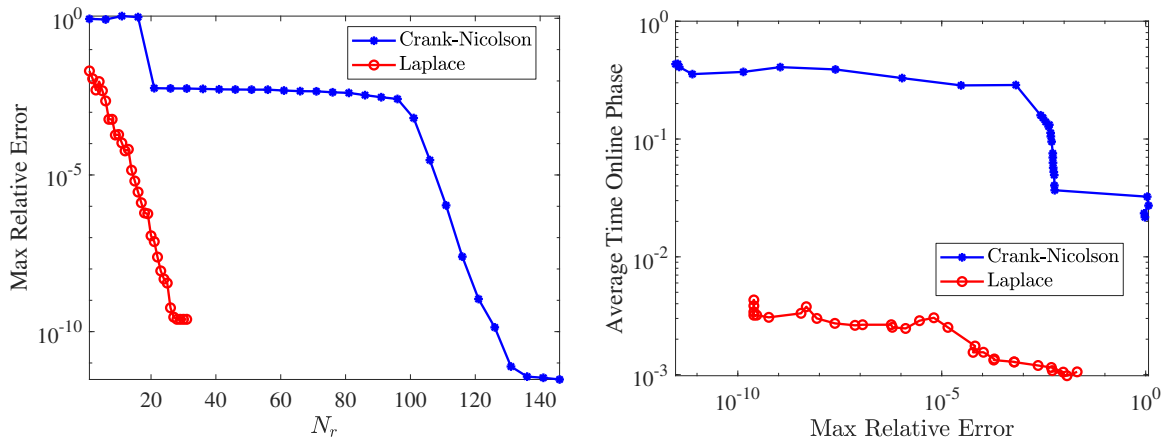


Figure 5: Black-Scholes test problem. Decay of the reduction error with respect to the reduced basis size (left) and computational time with respect to the reduction error (right) for the Crank-Nicolson method and the contour integral method. Time window $[0.1, 1]$ and $|\Xi| = 400$ uniformly distributed samples.

Methods	$\tilde{\sigma}$	$\frac{\tilde{\sigma} - \tilde{\sigma}_{LB}}{\tilde{\sigma}_{LB}}$	$\#SEP$	Time
GS	$3.3 \cdot 10^{-4}$	$-2.0 \cdot 10^{-3}$	111	1.29
SCM	$3.1 \cdot 10^{-7}$	$-9.9 \cdot 10^{-1}$	190	> 400
RBFI	$3.3 \cdot 10^{-4}$	$1.9 \cdot 10^{-11}$	332	55.8

Table 2: Black-Scholes test problem. Comparison among the three different strategies to determine $\tilde{\sigma}_{LB}$.

domain. The ability to compute the exact value is due to the fact that the lower bound is attained on a vertex of the parametric domain. In Table 2 we compare the gradient strategy with the SCM method [20, 4, 15] and the strategy based on RBFI [25]. To simplify we consider the matrix arising from the discretization in space of Black-Scholes operator, i.e.

$$\mathcal{A}u = \frac{1}{2}\sigma^2 s^2 \frac{\partial^2 u}{\partial s^2} + rs \frac{\partial u}{\partial s} - ru.$$

4.2 The Heston equation

The Heston equation [16] is a 2D convection diffusion equation given by

$$\frac{\partial u}{\partial \tau} = \frac{1}{2}s^2v \frac{\partial^2 u}{\partial s^2} + \rho\sigma sv \frac{\partial^2 u}{\partial s \partial v} + \frac{1}{2}\sigma^2v \frac{\partial^2 u}{\partial v^2} + (r_d - r_f)s \frac{\partial u}{\partial s} + \kappa(\eta - v) \frac{\partial u}{\partial v} - r_d u. \quad (31)$$

The unknown function $u(s, v, \tau)$ represents the price of a European option when at time $t - \tau$ the corresponding asset price is equal to s and its variance is v . We consider the equation on the

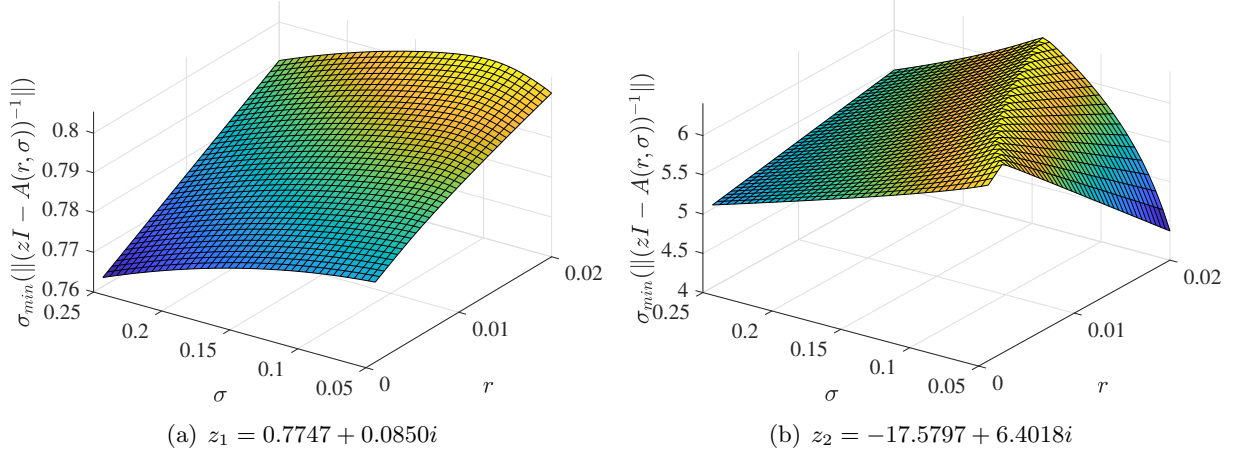


Figure 6: Black-Scholes test problem. Computed smallest singular value for each parameter in Ξ and in two quadrature points.

z	$\tilde{\sigma}_{GS}$	$\tilde{\sigma}_{LB}$	$\frac{\tilde{\sigma}_{GS} - \tilde{\sigma}_{LB}}{\tilde{\sigma}_{LB}}$	$\#SEP$
$0.4190 + 0.0803i$	0.4093	0.4093	0	21
$-3.6612 + 2.3961i$	1.4558	1.4558	0	22
$-9.4930 + 3.5718i$	2.0782	2.0782	0	22
$-17.3555 + 4.4742i$	2.4755	2.4755	0	22

Table 3: Black-Scholes test problem. Approximations of $\tilde{\sigma}_{LB}$ through the gradient type method. The table reports the relative error in the approximation and the number of solved eigenvalue problems (SEP) to compute the approximation $\tilde{\sigma}_{GS}$. The results are shown for 4 quadrature points z .

unbounded domain

$$0 \leq \tau \leq t, \quad s > 0, \quad v > 0,$$

where the time t is fixed. The parameters $\kappa > 0$, $\sigma > 0$, and $\rho \in [-1, 1]$ are given. Moreover equation (31) is usually considered under the condition $2\kappa\eta > \sigma^2$ that is known as the Feller condition (see [22]). We take equation (31) together with the initial condition

$$u(s, v, 0) = \max(0, s - K),$$

where $K > 0$ is fixed a priori (and represents the strike price of the option), and boundary condition

$$u(L, v, \tau) = 0, \quad 0 \leq \tau \leq t.$$

For the numerical solution of (31), we need to choose a bounded domain of integration, and follow [18]. In particular, we fix two positive constants S, V and we let the two variables s, v vary in the set

$$0 \leq s \leq S, \quad 0 \leq v \leq V.$$

On the new boundary, we need to add two more conditions (specific for the European call option),

$$\begin{aligned} \frac{\partial u}{\partial s}(S, v, \tau) &= e^{-r_f \tau}, \quad 0 \leq \tau \leq t, \\ u(s, V, \tau) &= s e^{-r_f \tau}, \quad 0 \leq \tau \leq t, \end{aligned}$$

which are treated analogously to the boundary condition in (29).

The spatial discretization we adopted is the one introduced in [18] with $N = 10^4$. We take $r_f = 0$, $K = 100$, $L = 0$, $S = 8K$, $V = 5$, we consider the time window $t \in [0.5, 1]$ and the parametric domain

$$(\sigma, r_d, \kappa, \eta, \rho)^T \in \mathcal{D} \equiv [0.18, 0.4] \times [0.001, 0.2] \times [1.2, 3] \times [0.08, 0.15] \times [0.21, 0.9].$$

We test the reduced basis approach for different dimension of the parameter domain $\mathcal{D} \subset \mathbb{R}^d$, $d=2, 5$, namely we consider $\mu = (\kappa, \eta)^T \in \mathbb{R}^2$ and $\mu = (\sigma, r_d, \kappa, \eta, \rho)^T \in \mathbb{R}^5$. For each choice of μ , the remaining parameter values are assumed to be fixed and taken from the default value parameter vector $\mu^* = (0.3, 0.02, 2, 0.1, 0.21)^T$. In our first test, we consider $\mu = (\kappa, \eta)^T$ and $|\Xi| = 15^2 = 225$ equidistantly distributed points. To quantify the efficiency of our reduced basis method, we investigate the error decay when increasing the dimension N_r . For each reduced model, we compute the maximal error as

$$E_r = \max_{\mu \in |\Xi|} \max_{t \in [0.5, 1]} \frac{\|u(t; \mu) - u_r(t; \mu)\|}{\|u(t; \mu)\|}. \quad (32)$$

In Figure 7 we illustrate the effectivity of our POD-Greedy algorithm based on the error estimator (24). Similar to the Black-Scholes problem, on the left plot, we see that the decay of absolute error is reproduced by the one of the error estimator, while, on the right plot, we observe the desired exponential decay of the relative error with respect to the reduced basis size. Analogous results for the other choice of $\mu = (\sigma, r_d, \kappa, \eta, \rho)^T$, that is the vectors of all parameters of the Heston

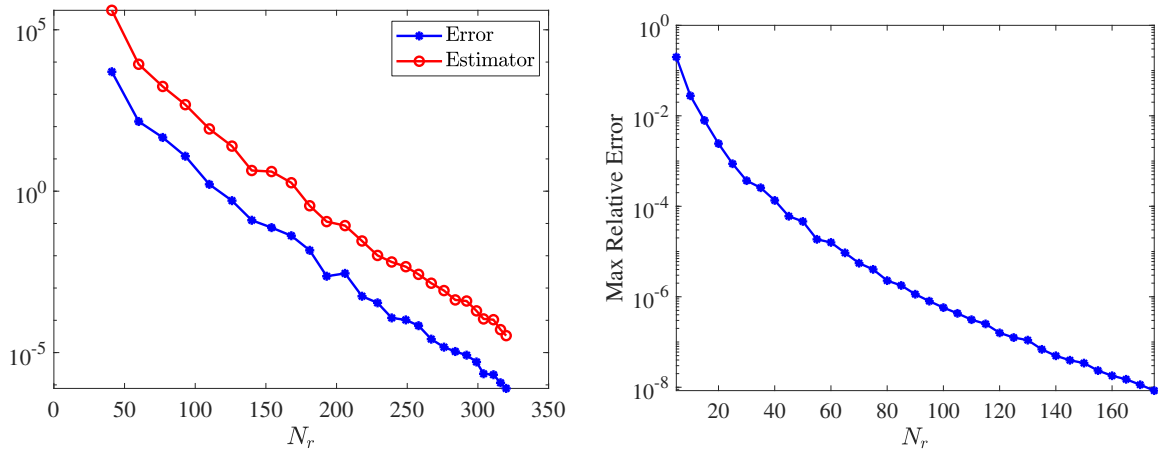


Figure 7: Heston test problem with $\mu = (\kappa, \eta)^T$. Behaviour of the Greedy-POD selection algorithm (left); decay of the relative error (32) with respect to the reduced basis size (right). The parametric train set is composed of $|\Xi| = 15^2$ equidistantly distributed points.

equation, are presented in Figure 8 where $|\Xi| = 5^5 = 3125$ equidistantly distributed points. We observe also in this case the exponentially decaying behaviour of the error. However note that the convergence is slower, which is explained by the increasingly complex parameter dependence of the model.

	$d = 2$		$d = 5$	
	CPU time (s)	# Stored Snapshots	CPU time (s)	# Stored Snapshots
Algorithm 1	618	320	18421	1115
Algorithm 2	944	811	14420	4848

Table 4: Heston test problem with $d = 2$ parameters and $d = 5$ parameters. CPU time and number of stored snapshots with the greedy-POD strategy of Algorithm 1 and the local greedy strategy of Algorithm 2.

In Table 4 and Figure 9 the performances of Algorithm 1 and Algorithm 2 for $d = 2$ and $d = 5$ are illustrated. The results confirm what observed for the Black-Scholes test problem, the local approach is more expensive in terms of computational time and number of stored snapshots while the decay of error with respect to the reduced basis is strongly improved. Again we conclude that the local approach is better suited for this problem due to the significant improvement in the accuracy reached in the online phase with respect to the reduced basis size.

Also for the Heston problem (for $\mu \in \mathbb{R}^2$) we compare the Laplace reduced basis method with the classical one based on the Crank-Nicolson time scheme (with $\Delta t = 10^{-4}$) over the time window $[0.5, 1]$. The error in the full time discretization is around 10^{-4} for Laplace and $5 \cdot 10^{-2}$ for Crank-Nicolson. Figure 10 compares the average CPU time for the solution of the reduced problem over

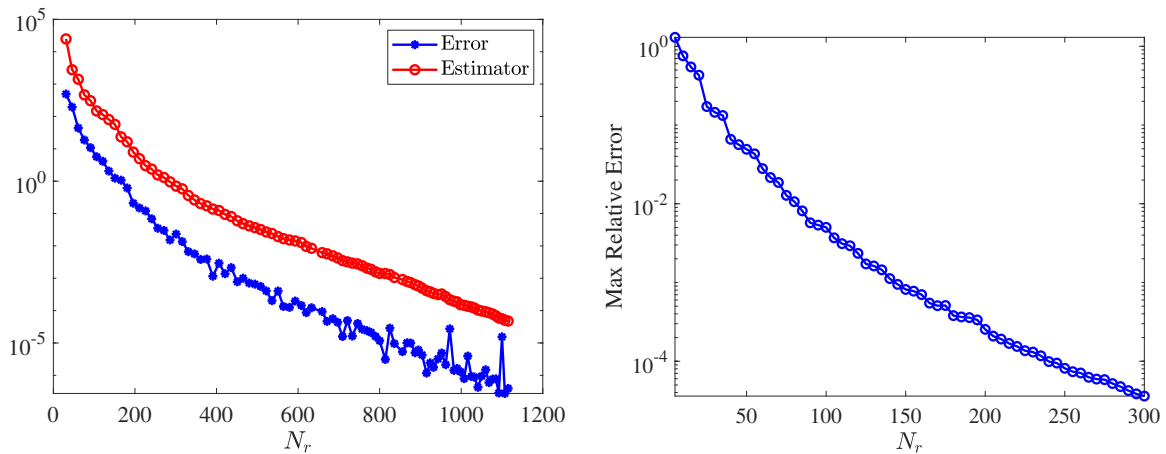


Figure 8: Heston test problem with $\mu = (\sigma, r_d, \kappa, \eta, \rho)^T$. Behaviour of the Greedy-POD selection algorithm (left); decay of the relative error (32) with respect to the reduced basis size (right). The parametric set is composed of $|\Xi| = 5^5$ equidistantly distributed points.

a test set of 100 uniformly randomly distributed values. The contour integral method is between 6 and 23 times faster than the classical Crank-Nicolson in the online phase.

Figure 11 (right) shows the behaviour of the relative error with respect to the size of the reduced basis for the two reduction techniques. The error originated by the Laplace reduced basis is always significantly smaller than the one associated to the classical reduced basis method. Figure 11 (left) compares the two reduction techniques in terms of computational time with respect to the associated reduction error. It can be seen that the Laplace reduced basis is around the two order of magnitude faster than the classical reduced basis method.

Finally in Table 5 are reported the results of our gradient based strategy for the computation of $\tilde{\sigma}_{LB}$ in the Heston problem with 5 parameters. The number of selected starting point is 32, while for the estimation of $\tilde{\sigma}_{LB}$ we make use of the discrete domain Ξ defined previously. It can be seen that with a maximum of 331 eigenvalues computations the method is able to approximate with high accuracy the lower bound on the parametric domain (and in some cases it recover smaller values than the ones associated to the discrete set Ξ). The number of eigenvalue problems solved increases considerably with respect to the Black-Scholes test problem (see Table 3); despite this fact we observe that the dimension of the parametric domain is much larger and that the cost of our procedure determines a strong speed up with respect to the direct evaluation on the discrete grid Ξ . Moreover the computed values coincide with the minimum over the continuum domain, which means that the discrete domain Ξ can be changed without the need to recompute the lower bound.

4.3 The advection equation

As last illustration of our method we apply it to the canonical one dimensional advection equation

$$u_t + \mu u_x = 0, \quad t \geq 0, \quad x \in [0, d], \quad (33)$$

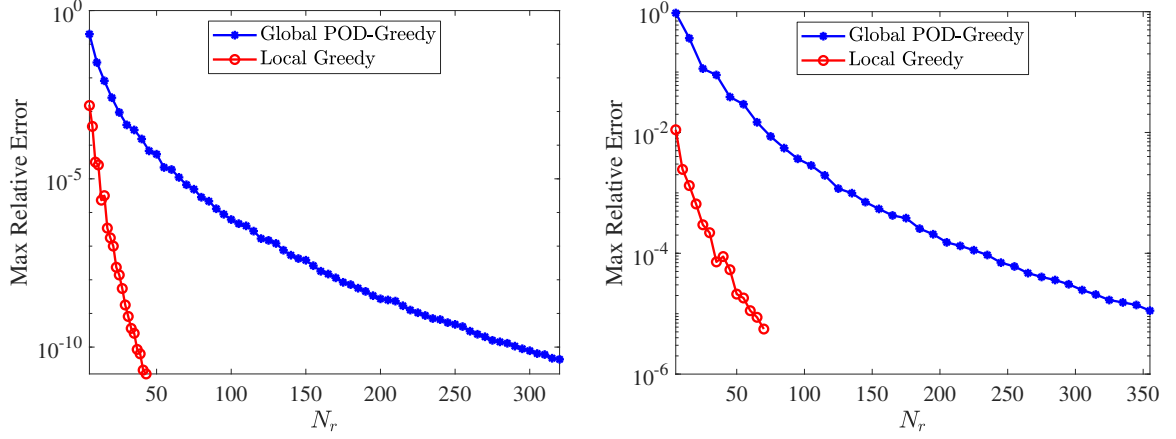


Figure 9: Heston test problem with $d = 2$ parameters (left) and $d = 5$ parameters (right). Decay of the error (32), with respect to the reduced basis size constructed with the POD-Greedy strategy (Algorithm 1) and the local Greedy one (Algorithm 2). Time window $[0.5, 1]$, $|\Xi| = 15^2$ for $d = 2$ (left) and $|\Xi| = 5^5$ for $d = 5$ (right) uniformly distributed samples.

z	$\tilde{\sigma}_{GS}$	$\tilde{\sigma}_{LB}$	$\frac{\tilde{\sigma}_{GS} - \tilde{\sigma}_{LB}}{\tilde{\sigma}_{LB}}$	$\#SEP$
$6.3125 + 0.6398i$	0.0958	0.0958	0	121
$4.0569 + 8.2377i$	3.5251	3.5234	0.0005	212
$-11.4305 + 21.8591i$	0.2101	0.2101	0	131
$-17.3254 + 24.6875i$	0.0633	0.0633	0	131
$-23.8980 + 27.2103i$	0.0164	0.0165	-0.0081	160
$-31.0669 + 29.3965i$	0.0026	0.0032	-0.1955	331

Table 5: Heston test problem. Approximations of $\tilde{\sigma}_{LB}$ through the gradient type method computed in 10 quadrature points z . The table reports the relative error in the approximation and the number of solved eigenvalue problems (SEP) to compute the approximation $\tilde{\sigma}_{GS}$.

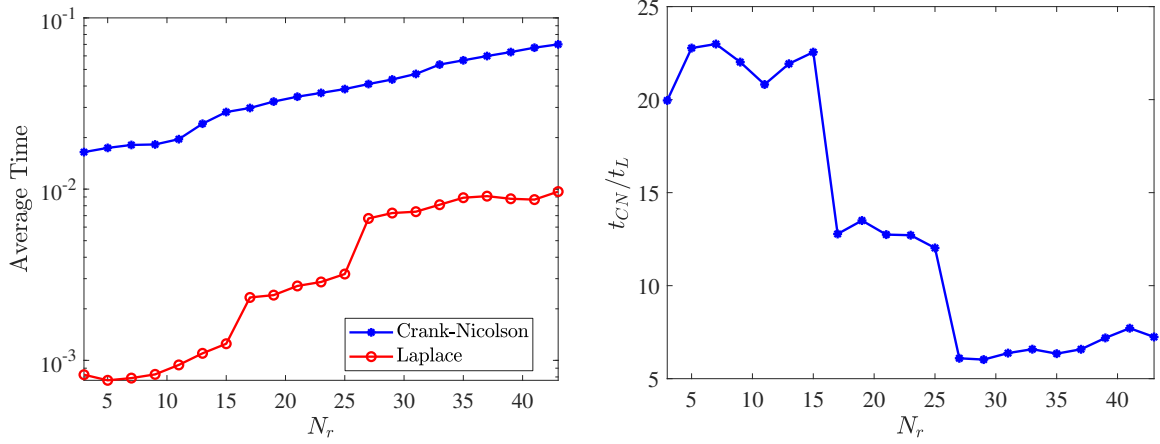


Figure 10: Heston test problem. Behaviour of the computational time with respect to the reduced basis size for Crank-Nicolson and Laplace. Direct comparison (left) and ration between the averages time (right).

with initial and boundary conditions

$$u(x, 0) = H(x - 0.2) = \begin{cases} 0 & x < 0.2 \\ 1 & 0.2 \leq x \leq d \end{cases}, \quad u(0, t) = 0, \quad u(d, t) = 1. \quad (34)$$

It has been shown, see [26], that for such a problem (33)-(34) the Kolmogorov N -width associated to the solution manifold originated by the map

$$\Phi : \quad \mu \longrightarrow H(x - 0.2 - \mu t),$$

has only a polynomial type decay, which suggests that reduced basis might be inappropriate.

We discretize in space (33) with an upwind scheme, setting $d = 1$ and $\Delta x = 10^{-3}$. For the time treatment and successive reduction procedure we compare our approach and the classical reduction based on a backward Euler scheme with stepsize $\Delta t = 10^{-3}$ and final time $T = 0.5$. For the parametric domain we set $\mu \in \mathcal{D} = [0.1, 1]$ and we build the training set Ξ_{train} taking $N_{train} = 20$ values of the velocity μ uniformly distributed in \mathcal{D} while for the test set Ξ_{test} we consider $N_{test} = 100$ uniformly randomly distributed values. Since the small size of the train set we do not use the greedy strategy for the computation of the reduced space, and we directly evaluate the full solution on all the train set. Then we build the space through POD decomposition.

Figure 12 shows that our reduction strategy is effective. The decay of the singular values, which, in some sense, mimics the behaviour of the Kolmogorov N -width [6], is faster. In order to validate our strategy we consider the relative error

$$E_r = \max_{\mu \in \Xi_{test}} \frac{\|u(T; \mu) - u_r(T; \mu)\|}{\|u(T; \mu)\|}, \quad (35)$$

that shows a decay behaviour similar to the one of the singular values.

Note the jump happening between the 500th and 501th singular value for the classical reduced basis

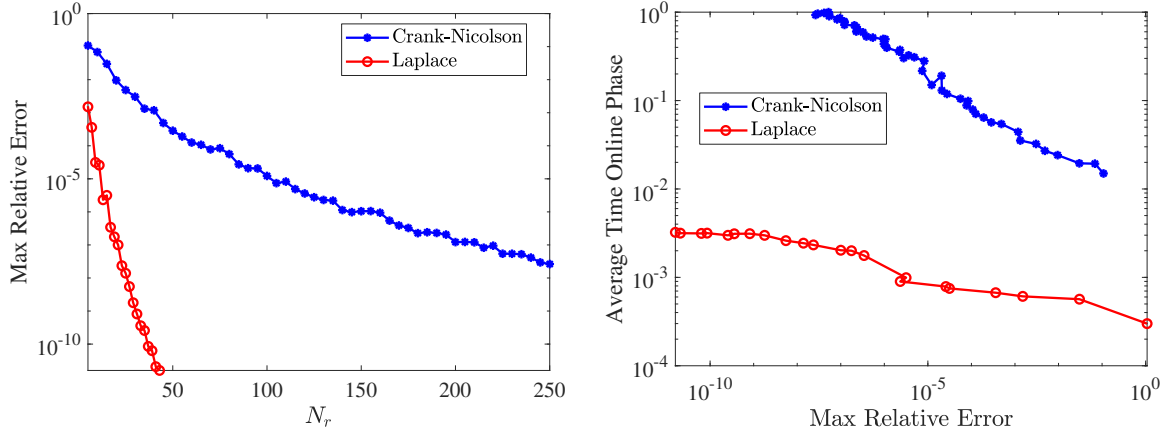


Figure 11: Heston test problem. Decay of the reduction error with respect to the reduced basis size (left) and computational time with respect to the reduction error (right) for the Crank-Nicolson method and the contour integral method. Time window $[0.5, 1]$ and $|\Xi| = 225$ uniformly distributed sample.

method. This is due to the presence of 500 step functions with different location of the discontinuity in the discrete solution manifold. Indeed, when taking the velocity $\mu = 1$ it holds

$$\mu \frac{\Delta x}{\Delta t} = 1,$$

which implies that if at time t_i the jump is located at x_i then at time $t_{i+1} = t_i + \Delta t$ the jump will be located at $x_{i+1} = x_i + \Delta x$. Since the final time is $T = 0.5$ and $\Delta t = 10^{-3}$, it follows the presence of exactly 500 step functions. The set of step functions is isomorphic to an orthogonal set of same size, for this reason the N -width has only an algebraic power decay (see [10]). This explains the jump in the blue line of Figure 12 (left); the decay of the magnitude of the singular values is slow until all the information related to the 500 step functions is included in the reduced space, then the jump tells us that all the other elements in the discrete solution manifold can be well approximated by the subset generated from the 500 step functions. The reason why our strategy is effective in dealing with the reduction of the advection problem is that the solution manifold (13) is defined on the Laplace transform domain where the step function becomes

$$\mathcal{L}(H(\mu t - a)) = \frac{1}{|\mu|} \frac{e^{-a \frac{s}{\mu}}}{s}, \quad a \in \mathbb{R},$$

which does not lead to a slow decay of the Kolmogorov N -width. We show this in Figure 13 where is reported the decay of the singular values associated to matrices built taking snapshots of $H(\mu t - x)$ and $\mathcal{L}(H(\mu t - a))$ for $\mu t \in [0.5, 5]$, $x \in [0, 1]$ and size of the discrete space domain $N_h = 1000$.

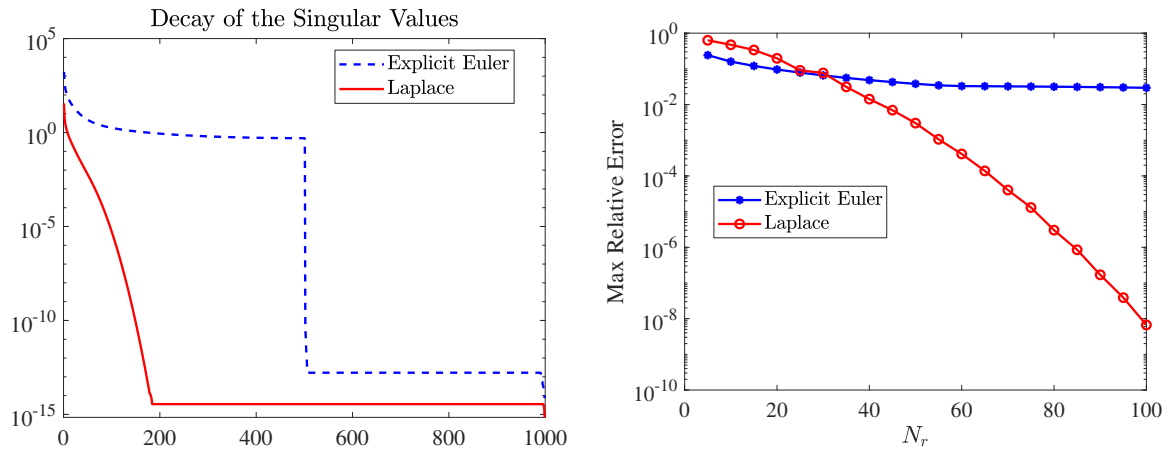


Figure 12: Linear 1D advection problem. Decay of the singular values (left) and of the error (35) (right).

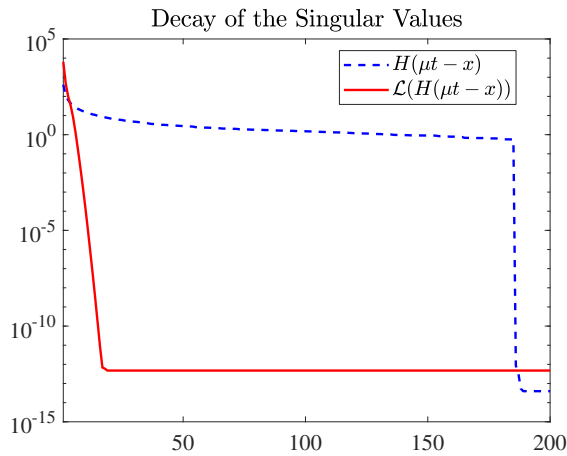


Figure 13: Decay of the singular values associated to the snapshots matrices of $H(\mu t - x)$ and $\mathcal{L}(H(\mu t - a))$ for $\mu t \in [0.5, 5]$ and $x \in [0, 1]$.

5 Conclusions

In this article we have presented a new approach, based on the coupling of contour integral methods and reduced basis methods to solve time dependent PPDEs. The main features of the proposed method which distinguish it from classical approaches and make it very efficient are summarized by the following:

- 1) the possibility to parallelize the computation of $\hat{u}(z)$ on the quadrature nodes and the construction of the reduced basis in the local greedy strategy;
- 2) the fact that the solution is computed for all times t in a suitable time window, that is also true at the level of the reduced problem;
- 3) an efficient treatment of linear hyperbolic problems with discontinuous initial data.

We have experimented our method on several numerical tests. The direct comparison with the reduction performed through the Crank-Nicolson time stepping scheme shows a faster decay of the reduction error of our method which led to a significant gain in computational time in the online phase

A Appendix

Let us write problem (1) as

$$\begin{aligned} G_1[u] &= \mathcal{A}(x; \mu)[u] + f(x, t; \mu), \\ G_1 &= \frac{\partial}{\partial t}, \\ u(x, 0; \mu) &= g(x; \mu). \end{aligned} \tag{36}$$

where for compactness we omitted the dependence of u from variables and parameters. We formally write the solution of (36) as the series

$$u(x, t; \mu) = \sum_{k=0}^{\infty} u_k(x, t; \mu). \tag{37}$$

By plugging (37) into (36), using the fundamental theorem of integral calculus, one has

$$\sum_{k=0}^{\infty} u_k(x, t; \mu) = u(x, 0; \mu) + \int_0^t \left(\mathcal{A}(x; \mu) \left[\sum_{k=0}^{\infty} u_k \right] + f(x, t; \mu) \right) d\tau. \tag{38}$$

After defining

$$u_0(x, t; \mu) = u(x, 0; \mu) + \int_0^t f(x, \tau; \mu) d\tau,$$

in order to determine the coefficients of the series we express the term of index k on the left hand side of (38) with the term of index $k - 1$ on the right hand side. Note that this is possible thanks to the linearity of \mathcal{A} and of the integration.

In doing so we get the recurrence relation

$$u_k(x, t; \mu) = \int_0^t \left(\mathcal{A}(x; \mu) [u_{k-1}(x, t; \mu)] \right) d\tau, \quad k \geq 1;$$

which, by linearity, can be made explicit in terms of u_0

$$u_k(x, t; \mu) = \mathcal{Q}^k \left[\mathcal{A}^k(x; \mu) [u_0(x, t; \mu)] \right],$$

where $\mathcal{Q}[u] = \int_0^t u \, d\tau$. Note that operators \mathcal{Q} and \mathcal{A} commute.

We denote by Y^* the subspace generated by the first n terms of (37), in general the dimension of Y^* is less or equal n , say for instance n^* . Recalling the definition of Kolmogorov N -width given in (11) we get

$$\begin{aligned} d_n(\mathcal{M}) \leq d_{n^*}(\mathcal{M}) &= \inf_{\dim(Y)=n^*} \sup_{u(\mu) \in \mathcal{M}} \inf_{v \in Y} \|u - v\|_{\mathbb{V}} \leq \sup_{u \in \mathcal{M}} \inf_{v \in Y^*} \|u - v\|_{\mathbb{V}} \\ &\leq \sup_{u \in \mathcal{M}} \left\| u(\mu) - \sum_{k=0}^{n-1} u_k(\mu) \right\|_{\mathbb{V}} = \sup_{u \in \mathcal{M}} \left\| \sum_{k=n}^{\infty} u_k(\mu) \right\|_{\mathbb{V}} \\ &\leq \sup_{u \in \mathcal{M}} \left\{ \sum_{k=n}^{\infty} \|u_k(\mu)\|_{\mathbb{V}} \right\}. \end{aligned} \quad (39)$$

Concerning $\|u_k(\mu)\|_{\mathbb{V}}$, for $t = T$, we have

$$\begin{aligned} \|u_k(\mu)\|_{\mathbb{V}} &= \left\| \mathcal{Q}^k \left[\mathcal{A}^k(x; \mu) [u_0(\mu)] \right] \right\|_{\mathbb{V}} \leq \mathcal{Q}^k \left[\|\mathcal{A}(\mu)\|_{\mathbb{V}}^k \|u_0(\mu)\|_{\mathbb{V}} \right] \\ &\leq \mathcal{Q}^k \left[\|\mathcal{A}(\mu)\|_{\mathbb{V}}^k (\|g(\mu)\|_{\mathbb{V}} + \mathcal{Q}[\|f(\mu)\|_{\mathbb{V}}]) \right] \\ &\leq \frac{(T \|\mathcal{A}(\mu)\|_{\mathbb{V}})^k}{k!} \left(\|g(\mu)\|_{\mathbb{V}} + M \frac{T}{k+1} \right), \end{aligned}$$

with $M = \sup_{\mu \in \mathcal{D}} \max_{t \in [0; T]} \|f(\mu)\|_{\mathbb{V}}$. For k large enough it exists $S(\mu) \in \mathbb{R}^+$ such that $S(\mu) > T \|\mathcal{A}(\mu)\|_{\mathbb{V}}$ and $k! > S(\mu)^k$, therefore

$$\|u_k(\mu)\|_{\mathbb{V}} \leq C_1(\mu) \left(\frac{T \cdot \|\mathcal{A}(\mu)\|_{\mathbb{V}}}{S} \right)^k = C_1(\mu) (1 - \varepsilon(\mu))^k, \quad (40)$$

with $C_1(\mu) = \|g(\mu)\|_{\mathbb{V}} + MT$. Substituting (40) into (39) we finally obtain

$$\begin{aligned} d_n(\mathcal{M}) &\leq \sup_{\mu \in \mathcal{D}} \left\{ C_1(\mu) \sum_{k=n}^{\infty} (1 - \varepsilon(\mu))^k \right\} = \sup_{\mu \in \mathcal{D}} \left\{ C_1(\mu) (1 - \varepsilon(\mu))^n \sum_{k=0}^{\infty} (1 - \varepsilon(\mu))^k \right\} \\ &= \sup_{\mu \in \mathcal{D}} \left\{ \frac{1}{\varepsilon(\mu)} C_1(\mu) e^{n \log(1 - \varepsilon(\mu))} \right\} \leq c_1 e^{-c_2 n}, \end{aligned}$$

where $c_1 = \sup_{\mu \in \mathcal{D}} \left(\frac{1}{\varepsilon(\mu)} C_1(\mu) \right)$ and $c_2 = \inf_{\mu \in \mathcal{D}} (-\log(1 - \varepsilon(\mu)))$.

References

- [1] M. Barrault, Y. Maday, N. C. Nguyen, and A. T. Patera. An ‘empirical interpolation’ method: application to efficient reduced-basis discretization of partial differential equations. *Comptes Rendus Mathématique*, 339(9):667–672, 2004.
- [2] P. Binev, A. Cohen, W. Dahmen, R. DeVore, G. Petrova, and P. Wojtaszczyk. Convergence rates for greedy algorithms in reduced basis methods. *SIAM Journal on Mathematical Analysis*, 43(3):1457–1472, 2011.
- [3] F. Black and M. Scholes. The pricing of options and corporate liabilities. *Journal of Political Economy*, 81(3):637–654, 1973.
- [4] Y. Chen, J. Hesthaven, Y. Maday, and J. Rodríguez. Improved successive constraint method based a posteriori error estimate for reduced basis approximation of 2d maxwell’s problem. *Mathematical Modelling and Numerical Analysis*, 43, 11 2009.
- [5] A. Cohen and R. DeVore. Kolmogorov widths under holomorphic mappings. *IMA Journal of Numerical Analysis*, 36(1):1–12, 03 2015.
- [6] S. M. Djouadi. On the optimality of the proper orthogonal decomposition and balanced truncation. In *2008 47th IEEE Conference on Decision and Control*, pages 4221–4226, Dec 2008.
- [7] M. Drohmann, B. Haasdonk, and M. Ohlberger. Reduced basis approximation for nonlinear parametrized evolution equations based on empirical operator interpolation. *SIAM Journal on Scientific Computing*, 34(2):A937–A969, 2012.
- [8] C. Farhat, T. Chapman, and P. Avery. Structure-preserving, stability, and accuracy properties of the energy-conserving sampling and weighting method for the hyper reduction of nonlinear finite element dynamic models. *Int. J. Numer. Meth. Engng*, 102(5):1077–1110, May 2015.
- [9] S. Glas, A. Mayerhofer, and K. Urban. *Two Ways to Treat Time in Reduced Basis Methods*, pages 1–16. Springer International Publishing, Cham, 2017.
- [10] C. Greif and K. Urban. Decay of the kolmogorov n-width for wave problems. *Applied Mathematics Letters*, 96:216 – 222, 2019.
- [11] N. Guglielmi, M. Lopez-Fernandez, and G. Nino. Numerical inverse laplace transform for convection-diffusion equations in finance. *Mathematics of Computation*, 89, 01 2018.
- [12] N. Guglielmi, M. López-Fernández, and M. Manucci. Pseudospectral roaming contour integral methods for convection-diffusion equations. *Journal of Scientific Computing*, 89(1):22, 2021.
- [13] B. Haasdonk. Convergence rates of the pod-greedy method. *ESAIM: Mathematical Modelling and Numerical Analysis*, 47(3):859–873, 2013.
- [14] J. Hesthaven, G. Rozza, and B. Stamm. *Certified Reduced Basis Methods for Parametrized Partial Differential Equations*. 01 2016.

- [15] J. S. Hesthaven, B. Stamm, and S. Zhang. Certified reduced basis method for the electric field integral equation. *SIAM Journal on Scientific Computing*, 34(3):A1777–A1799, 2012.
- [16] S. L. Heston. A closed-form solution for options with stochastic volatility with applications to bond and currency options. *Rev Financ Stud*, 6(2):327–343, April 1993.
- [17] R. A. Horn and C. R. Johnson. *Matrix Analysis*. Cambridge University Press, Cambridge, 1985.
- [18] K. Hout and S. Foulon. Adi finite difference schemes for option pricing in the heston model with correlation. *International Journal of Numerical Analysis and Modeling*, 7, November 2008.
- [19] K. Hout and J. Weideman. A contour integral method for the black–scholes and heston equations. *arXiv.org, Quantitative Finance Papers*, 33, 12 2009.
- [20] D.B.P. Huynh, G. Rozza, S. Sen, and A.T. Patera. A successive constraint linear optimization method for lower bounds of parametric coercivity and inf–sup stability constants. *Comptes Rendus Mathematique*, 345(8):473–478, 2007.
- [21] K. J. in 't Hout and B. D. Welfert. Stability of adi schemes applied to convection-diffusion equations with mixed derivative terms. *Applied Numerical Mathematics*, 57(1):19–35, 2007.
- [22] A. Janek, T. Kluge, R. Weron, and U. Wystup. Fx smile in the heston model. In Pavel Cizek, Wolfgang Karl Härdle, and Rafał Weron, editors, *Statistical Tools for Finance and Insurance*, pages 133–162. Springer Berlin Heidelberg, Berlin, Heidelberg, 2011.
- [23] T. Kato. *Perturbation theory for linear operators*, volume 132. Springer Science & Business Media, 2013.
- [24] M. Manucci, J. Vicente Aguado, and D. Borzacchiello. Sparse data-driven quadrature rules via ℓ^p -quasi-norm minimization. *ArXiv*, abs/2012.05264, 2020.
- [25] A. Manzoni and F. Negri. Heuristic strategies for the approximation of stability factors in quadratically nonlinear parametrized pdes. *Advances in Computational Mathematics*, 41, 10 2015.
- [26] M. Ohlberger and S. Rave. Reduced basis methods: Success, limitations and future challenges. 11 2015.
- [27] C. Prud'homme, D. V. Rovas, K. Veroy, L. Machiels, Y. Maday, A. T. Patera, and G. Turinici. Reliable real-time solution of parametrized partial differential equations: Reduced-basis output bound methods. *J. Fluids Eng*, 124(1):70–80, November 2001.
- [28] L. Sirovich. Turbulence and the dynamics of coherent structures. i - coherent structures. ii - symmetries and transformations. iii - dynamics and scaling. *Quarterly of Applied Mathematics - QUART APPL MATH*, 45, 10 1987.

- [29] L. N. Trefethen and M. Embree. *Spectra and Pseudospectra: The Behavior of Nonnormal Matrices and Operators*. Princeton University Press, 2005.
- [30] K. Urban and A. T. Patera. A new error bound for reduced basis approximation of parabolic partial differential equations. *Comptes Rendus Mathematique*, 350(3):203 – 207, 2012.
- [31] M. Yano and A. T. Patera. An lp empirical quadrature procedure for reduced basis treatment of parametrized nonlinear pdes. *Computer Methods in Applied Mechanics and Engineering*, 344:1104–1123, 2019.